Upstream Effects of Mesoscale Mountains[1]

R. T. PIERREHUMBERT AND B. WYMAN

Geophysical Fluid Dynamics Laboratory, NOAA, Princeton, NJ 08542

(Manuscript received 29 August 1984, in final form 2 January 1985)

ABSTRACT

The Alpine Experiment (ALPEX) has revealed that low-level air is typically diverted around the Alps without reaching the mountaintop. In pursuit of an understanding of the physical basis of this phenomenon and of its generality, we have explored the characteristics of orographic blocking of a rotating continuously stratified fluid, as revealed in a simple model problem retaining full nonlinear and transient effects. Hydrostatic dynamics is assumed, and the obstacle is taken to be an infinitely long ridge with height $h(x)$. The key questions treated are the strength of the upstream deceleration of cross-mountain flow and the length scale over which the decelerated region extends. By means of scale analysis, the controlling parameters are found to be the Rossby number $\mathrm{Ro} = U/fL$ and the Froude number $\mathrm{Fr} = Nh_m/U$, where U is the speed of the oncoming flow, f is the Coriolis parameter, L the mountain half-width, N the Brunt–Väisälä frequency, and h_m is the maximum mountain height. The scale analysis also determines the qualitative dependence of the strength of the blocking on Ro and Fr; these predictions were confirmed and made quantitative via extensive numerical simulation.

In the nonrotating limit, Fr is the sole parameter. In this case, it is found that for sufficiently large Fr a decelerated layer of fluid forms near the obstacle and propagates arbitrarily far upstream with time, in a manner similar to that familiar in one-layer hydraulic theory. The upstream influence requires neither downstream lee wave trains nor vertical confinement by a rigid lid; rather, the upstream modes appear to be generated by wave breaking above the lee slope of the mountain. For a Gaussian mountain profile, wave breaking and upstream influence set in near $\mathrm{Fr} = 0.75$; low-level flow upstream of the mountain is decelerated to rest for $\mathrm{Fr} > 1.5$. In the rotating case, the decelerated zone does not propagate infinitely far. Instead, it attains a maximum extent on the order of the radius of deformation Nh_m/f before retreating toward the mountain. The upstream scales remaining after a long time has passed are also discussed.

The theory accounts for a number of aspects of the ALPEX data, as well as for features seen in earlier observations of barrier winds elsewhere. It appears though that the sharp transition between flow over and flow around found in certain ALPEX vertical soundings obtained from aircraft cannot be explained in terms of inviscid theory. It is conjectured that the sharp division is due to low-level convective mixing.

1. Introduction

One of the most striking features revealed by the Alpine Experiment (ALPEX) was the sharp division between currents below mountain-top level, which flow predominantly around the Alps, and those above mountain-top level, which cross the mountain barrier with little evidence of orographic perturbation. This pattern was observed on a number of occasions and under a variety of different synoptic situations. A particularly clear-cut instance of the phenomenon is evidenced in the set of aircraft soundings from flight E430 on 30 April 1982, shown in Fig. 1, as adapted from the Quick-Look microfilm archives. These soundings were taken at three points along the northern edge of the Alps, approximately 100 km north of the ridge line. The ambient far-upstream flow at this time was generally northerly at all levels. At 9 and 10°E one sees a sharp shift in wind direction from generally northerly above 3000 m altitude to generally westerly below 3000 m. This height corresponds roughly to mountain-top level. Sharp shifts in the wind speed are also noted. At 8°E, towards the western edge of the Alps, the directional shift is also seen, but the winds become essentially stagnant at low levels. This is the "flow splitting" point; farther to the west air flows around the mountains to the right rather than to the left.

The blocking of low-level flow described above is likely to be an essential feature of flow in the vicinity of steep mountains. As such it would participate in virtually all other important orographic effects, including lee cyclogenesis, gravity wave generation and frontal distortion. It has obvious implications for the initialization of numerical models in mountainous terrain. Accordingly, an understanding of the physical basis of the phenomenon is of utmost importance. Several key questions emerge: Under what range of

[1] A preliminary version of this work was presented at the Fifth Course on Meteorology of the Mediterranean, held in Erice, Italy, May 1983 (Pierrehumbert, 1985a).

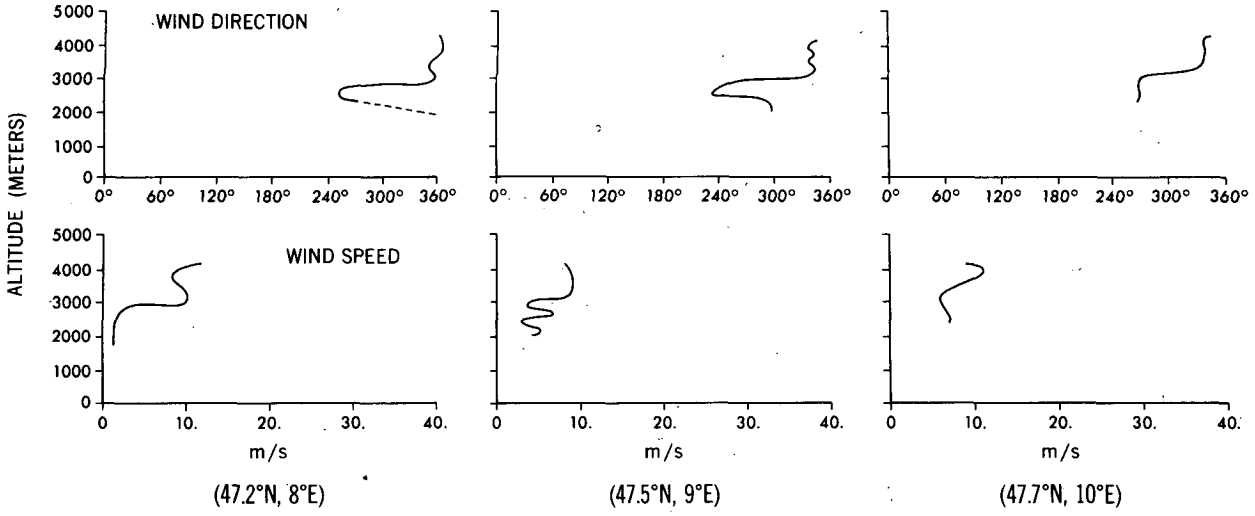

FIG. 1. Aircraft soundings of wind direction and speed taken approximately 100 km upwind of the Alps on 30 April 1984. Wind directions which are unreliable owing to low wind speeds are shown as dashed lines. See text for details.

atmospheric circumstances and for what orographic heights and steepnesses does the blocking occur? What are the controlling nondimensional parameters? How long does it take for the pattern to become established? How far upstream does the blocked region extend, and how deep is it? What role, if any, does the Coriolis force play in the phenomenon? In the present work, we endeavor to provide some answers to these questions. The emphasis will be on the fundamental physics governing the upstream pattern, as revealed in an idealized model; a detailed analysis of cases of upstream blocking observed during ALPEX and their simulation in more realistic models will be given in a future paper.

Intuitively, one would expect low-level dense air to be blocked by a sufficiently high mountain, provided the air is not moving too swiftly. Upstream influence of this sort is well known in the context of a single layer of fluid impinging on an obstacle in a nonrotating system. In the real continuously stratified atmosphere, however, the upstream blocking must overcome vertical dispersion, Coriolis force, and horizontal dispersion arising from three dimensionality. In the following, we address ourselves primarily to the implications of vertical dispersion and Coriolis force, though our results will enable us to draw some simple inferences concerning the likely three-dimensional flow patterns. Specifically, we consider the upstream effects attendant upon impulsive initiation of continuously stratified flow over an infinite ridge $h(x)$ on the rotating earth. The atmosphere is taken to be unbounded in the vertical. This problem is among the canon of fundamental problems of classical fluid dynamics; yet, the current understanding of the behavior of the solutions leaves much to be desired. Our main tool for investigating the system will be numerical simulation, buttressed by simple theoretical and physical arguments offered in explanation of the results. It will be seen that despite the limiting factors a blocked region can form upstream of the mountain when suitable conditions are met.

The upstream flow patterns of concern to us may be divided into three categories: 1) steady motions remaining a long time after flow is initiated, which decay in space with increasing distance from the obstacle, 2) transient motions which are created by the startup, but which decay to zero in any fixed spatial region given sufficient time, and 3) transient motions which form near the obstacle as a result of the initiation process and lead to order unity modifications of the upstream flow which extend progressively farther upstream of the obstacle without diminution of amplitude as time passes. Motions of the latter type are commonly denoted by the term "upstream influence." In the nonrotating case, there is still considerable dispute concerning the circumstances under which upstream influence can occur in a continuously stratified fluid; hence, we will treat this case in detail. It will be seen that Coriolis forces prevent the occurrence of true upstream influence, though the blocked region can temporarily extend quite far upstream when the Coriolis forces are small.

The structure of the paper is as follows. In Section 2 we present the equations of motion and identify the nondimensional parameters. Scale analysis is used to determine the qualitative dependence of the solution on these parameters. In Section 3 we review previous numerical work on the problem and describe the numerical model used in our simulations. Section 4 treats upstream influence in nonrotating fluids; a historical review of the outstanding issues is given in Section 4a and numerical results addressing these issues are given in Section 4b. Results concerning modification of the initial upstream surge by Coriolis

forces are presented in Section 5. In Section 6 we describe the characteristics of the motions remaining in the system at very long times after the impulsive startup. In particular we compare the asymptotically steady solutions found at low Rossby numbers with analytic results based on the semigeostrophic approximation (Merkine, 1975; Pierrehumbert, 1985b). Some speculations concerning three-dimensional and dissipative effects are discussed in Section 7, along with applications of the theory to the Alpine problem and to the representation of mountains in numerical models. Our principal conclusions are summarized in Section 8.

2. Scale analysis of the model problem

Consider flow of a Boussinesq stratified fluid on the f-plane over an infinite ridge with height $h(x)$, as depicted in Fig. 2. Let u, v, and w be the velocity components in the x, y and z directions. We assume that at time $t = 0$ the velocity field is a potential flow with uniform value U in the x direction far from the obstacle; this corresponds to impulsively started flow. Suppose also that the Brunt–Väisälä frequency initially has constant value $N = (-g\partial_z\rho/\rho_0)^{1/2}$, where ρ_0 is the constant mean density. A radiation condition is imposed at $z = \infty$, and it is assumed that the scales of motion are such that the hydrostatic approximation is valid. This is a nonlinear version of the problem first studied by Queney (1947) and used in our earlier work (Pierrehumbert, 1984) to estimate the magnitude of steady-state deceleration appearing upstream of mountains. It is convenient to nondimensionalize horizontal distances by the length scale L of the mountain and vertical distances by the deformation depth $D = fL/N$, where f is the Coriolis parameter. Velocities are scaled by U, time by L/U, pressure by $\rho_0 fLU$ and density by $\rho_0 NfL/g$. In these units the equations of motion become

$$\mathrm{Ro}(du/dt) = v - \partial_x p, \tag{2.1}$$

$$\mathrm{Ro}(dv/dt) = 1 - u, \tag{2.2}$$

$$d\rho/dt = 0, \tag{2.3}$$

$$\partial_z(\mathrm{Ro}\cdot p) = -\rho \tag{2.4}$$

$$\partial_x u + \partial_z w = 0, \tag{2.5}$$

where $d/dt = \partial_t + u\partial_x + w\partial_z$ and $\mathrm{Ro} = U/fL$ is the cross-mountain Rossby number. The term "1" on the right-hand side of (2.2) represents the meridional pressure gradient that balances the incident geostrophic wind. In nondimensional units, the initial conditions on velocity and density far upstream of the mountain are

$$u = 1, \tag{2.6}$$

$$\rho = -z. \tag{2.7}$$

Thus far, the only free parameter that has appeared in the problem is Ro. For a given mountain shape with maximum dimensional height h_m, the only remaining free parameter is the nondimensional mountain height $h_m/D = (N/f)(h_m/L)$. This is the square root of a Burger number, and may also be written RoFr, where $\mathrm{Fr} = Nh_m/U$. Thus, the nonlinear Queney problem is completely controlled by Ro and Fr. It is our plan to investigate the general character of the flow as a function of these two parameters. We will be especially interested in how small u becomes immediately upstream of the mountain, as this characterizes the strength of the blocking effect of the mountain.

Consider first the case of small Ro. If u is order unity or less and motions with time scales faster than L/U have had time to decay, then the left-hand side of (2.1) is negligible. The wind parallel to the mountain is then geostrophically balanced. With this approximation (2.1)–(2.7) reduces to the semigeostrophic

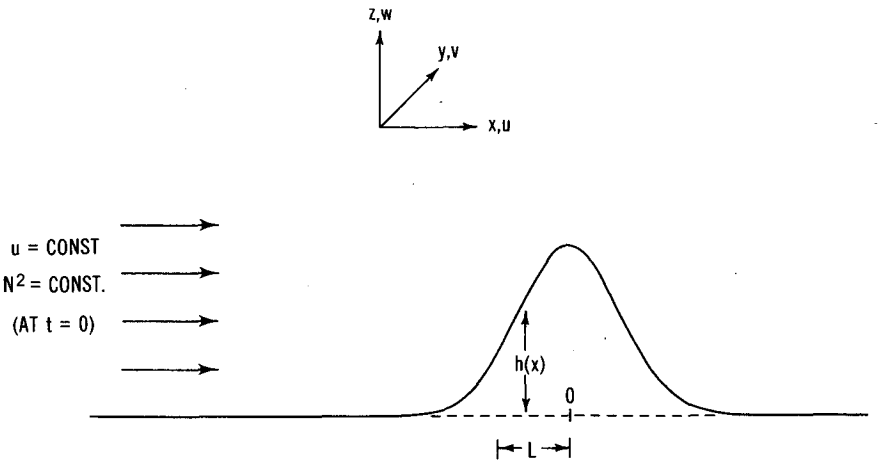

FIG. 2. Geometry of the model problem. The domain is taken to be unbounded in z, and the system is assumed to be rotating about the z axis with constant Coriolis parameter f.

system, steady solutions of which were discussed by Merkine (1975) and Pierrehumbert (1985b). Substituting $v = \partial_x p$ into (2.2) we find

$$(d/dt)[\partial_x(\mathrm{Ro}\cdot p)] = 1 - u. \tag{2.8}$$

Since Ro now appears only in the combination $\mathrm{Ro}\cdot p$, it can be absorbed into the definition of pressure, whence we find that the single parameter RoFr determines the character of the flow.

From (2.8) we can derive an estimate of the magnitude of u. When a parcel is displaced in the vertical by a nondimensional height δz, a density anomaly on the order of δz is created by virtue of (2.7). If D_1 is the dimensional depth scale over which this mountain-induced displacement vanishes, then (2.4) implies that $(\mathrm{Ro}\cdot p) \sim (D_1/D)\delta z$, whence (2.8) implies $(1 - u) \sim (D_1/D)\delta z$. Near the ground δz is approximately the nondimensional mountain height RoFr, provided that sufficient time has passed to allow fluid to reach the mountain top. For mountains of small height, the deformation depth D is the only dynamically relevant depth scale, whence $D_1/D = 1$. For high mountains, h_m could also enter as a depth scale, yielding $D_1/D = \mathrm{RoFr}$. Thus, $(1 - u)$ lies between O(RoFr) and O[(RoFr)^2]. In either case, u will deviate greatly from its upstream geostrophic value of unity when RoFr $\geqslant$ O(1) but will remain nearly undisturbed when RoFr $\ll 1$. This result is consistent with the behavior found in steady semi-geostrophic and quasigeostrophic flow (Pierrehumbert 1984, 1985b). The regime of validity of *quasi*-geostrophic theory is defined by RoFr $\ll 1$. Note that $\mathrm{RoFr} = (N/f)(h_m/L)$ is independent of the speed of the oncoming flow, so that if the slope of the mountain is too great the flow will never be quasi-geostrophic, no matter how small Ro may be.

As flow approaches the mountain, the isentropes must begin to rise, whence the pressure for fixed z increases; geostrophic balance then requires that v become positive as the mountain is approached. If v vanishes far upstream, (2.2) then implies that $(1 - u)$ becomes positive as the mountain is approached. Thus, the fluid slows down, becomes subgeostrophic, and turns to the left as it approaches the mountain from the upstream side. The scale analysis then implies that when Ro $\ll 1$ the blocking effect of the mountain becomes strong when RoFr $\geqslant$ O(1).

If the flow is impulsively started, the balanced solution described above will not be established until a dimensional time of $O(1/f)$ has passed. Nondimensionally, the adjustment time is O(Ro). During this time parcels near the ground move a nondimensional distance Ro in the horizontal and $\mathrm{Ro}\cdot(\mathrm{RoFr})$ in the vertical as they ascend the upwind slope. Equations (2.7) and (2.4) then imply that $\delta p \sim (D_1/D)\mathrm{RoFr}$. Substituting this into (2.1), integrating over a time interval Ro and making use of the assumption that v does not cancel the pressure gradient during this time, we find that $\delta u \sim -(D_1/D)\mathrm{RoFr}$. Three length scales could enter into the determination of D_1: the gravity wave scale U/N, the deformation depth D and the mountain height h_m. The first of these can be discarded, as group velocity arguments imply that at small Ro there is insufficient time to set up a gravity wave. We expect D to dominate for low mountains and h_m to dominate for higher mountains. In either case, the maximum deceleration appearing during the initial adjustment stage becomes order unity when RoFr becomes order unity. At small Ro then, the deceleration in the adjustment stage obeys the same scaling law as the deceleration in the balanced state, even though the adjustment stage is ageostrophic.

Finally, we estimate the magnitude of the deceleration at large Ro. Equations (2.1)–(2.4) may be rewritten

$$du/dt = -\partial_x(p/\mathrm{Ro}) + O(1/\mathrm{Ro}), \tag{2.9}$$

$$dv/dt = O(1/\mathrm{Ro}), \tag{2.10}$$

$$d(\rho/\mathrm{Ro})/dt = 0, \tag{2.11}$$

$$\mathrm{Ro}\partial_z(p/\mathrm{Ro}) = -\rho/\mathrm{Ro}. \tag{2.12}$$

Then, if we introduce a new pressure variable $p_1 = p/\mathrm{Ro}$, a new density variable $\rho_1 = \rho/\mathrm{Ro}$ and a new depth variable $z_1 = z/\mathrm{Ro}$, the appearance of Ro is eliminated from the system, to the extent that the O(1/Ro) terms are negligible. Note also that the upstream boundary condition on density becomes $\rho_1 = -z_1$ in the new units. The symbol z_1 is given in terms of the dimensional altitude z^* by $z_1 = (N/U)z^*$, whence the nondimensional mountain height is $\mathrm{Fr} = Nh_m/U$. Now, if a parcel is displaced in the vertical by a nondimensional distance Fr, and if the displacement remains coherent over a nondimensional depth ND_1/U, then hydrostatics implies a nondimensional pressure gradient of order $(ND_1/U)\mathrm{Fr}$ with high pressure appearing on the upwind slope of the mountain. According to (2.9), this leads to a deceleration of u on the order of $(ND_1/U)\mathrm{Fr}$. If $D_1 = U/N$ the deceleration is O(Fr), while $D_1 = h_m$ leads to a deceleration of O(Fr^2). We expect the former scaling to be valid in the linear range Fr $\ll 1$, where the mountain height does not provide a dynamically relevant depth scale. In any event, the argument implies that the deceleration becomes order unity when Fr becomes order unity.

An important caveat attaching to the above argument is that the large Ro approximation is not uniformly valid in space and time; given enough distance over which to act, the O(1/Ro) terms in (2.9)–(2.12) can yield order unity effects. This was discussed quantitatively for linear steady theory in Pierrehumbert (1984), and we shall have more to say about the matter in Section 5. In addition, the scale analysis at best estimates the deceleration im-

mediately upstream of the mountain; it tells us nothing about true upstream influence in the sense defined in Section 1.

A few comments on the nomenclature for the parameter Nh_m/U are in order. There seems to be no general agreement in the literature as to the name of this nondimensional number. The term "Froude number" is often used for its reciprocal U/Nh_m; this notation is consistent with the definition of Froude number for one-layer flow in the sense that the fluid velocity appears in the numerator (see Section 4a). Less frequently, the term "Froude number" is used for Nh_m/U itself; it is this terminology that we have implicitly adopted in defining $\mathrm{Fr} = Nh_m/U$. We prefer this definition because small Fr (in the nonrotating case) corresponds to the linear regime, so that Fr may be thought of as an expansion parameter. Readers who are more comfortable with the orthodox notation may think of Fr as standing for "reciprocal Froude number."

3. Description of numerical model

The mathematical difficulty of the problem is such that further progress cannot be made without recourse to numerical simulation. There has been a great deal of work on simulation of mountain waves in the nonrotating system (e.g., Peltier and Clark, 1979; Lilly and Klemp, 1979). This work has generally focused on the wave motions appearing above and downstream of mountains, and the effects of these waves on downslope wind storms. None of the studies treat the upstream effects in any detail. There has been less work on the simulation of the rotating problem. The first numerical solutions were accomplished by Eliassen and Rekustad (1971), who discussed only two cases, both of which involved rather broad and low mountains, and restricted attention to steady motion; further results with a similar model are reported in Eliassen and Thorsteinsson (1984). A number of other simulations of isolated cases have subsequently been reported (e.g., Parish, 1982), but the most systematic studies to date are those of Mason and Sykes (1978, 1979). The latter authors emphasize viscous and form drag effects, and do not discuss upstream deceleration or transience in any great detail. The interpretation of their results is complicated by the use of cyclic horizontal boundary conditions. In the present work we explore a much more extensive range of parameter space than any of the earlier studies. In Section 7 we will discuss some of the previous numerical results within the framework developed herein.

Our simulations were carried out using a slight modification of the two-dimensional (x, z) dry, hydrostatic primitive equation model described in Orlanski and Ross (1977). The model incorporates open horizontal boundary conditions which allow motions with well-defined phase speeds to propagate out of the domain without affecting the interior. An important feature of the model is a parameterized vertical diffusivity of mass, vorticity and y-momentum which is essentially zero in statically stable regions but becomes large as the lapse rate becomes statically unstable. This common expedient allows wave breaking to be handled without explicitly resolving convective mixing; it may be viewed as a surrogate for convective adjustment. A free-slip boundary condition is used at the ground, eliminating complicating boundary layer effects. We modified the model as follows:

1) Mountains were incorporated via a terrain-following coordinate system $s = H[z - h(x)]/[H - h(x)]$, where H is the height of the model lid. Except where otherwise noted we used a Gaussian mountain $h = h_m \exp(-x^2/L^2)$.

2) A sponge layer was introduced at the top of the domain to prevent reflection of energy from the lid. In this layer winds and densities were made to relax toward their initial values with a damping constant that ranged from zero at the bottom of the sponge layer to its maximum value at the top. Tests against known linear solutions indicated the spurious reflection to be very small. Some tests in the nonlinear range are discussed in Sections 4 and 5.

3) The model was made Boussinesq by replacing all densities by a constant except in the buoyancy term.

4) A weak biharmonic horizontal diffusion was added in order to damp two-grid noise that was sometimes created by wave breaking. The coefficient was chosen so as to have negligible effect on the large scale.

All results will be presented in terms of nondimensional units with velocity scale U, length scale L, time scale L/U and depth scale U/N. On some plots, the original dimensional units for which the calculation was carried out are also indicated. The horizontal grid length was held fixed at 0.2 units for all runs. Except where otherwise indicated, the domain extends ten units upstream and downstream of the mountain peak. Because some problems were occasionally noted with spurious reflection from the horizontal boundaries, calculations were generally terminated when high-amplitude motions arrived at either boundary. A nonuniform grid with maximum resolution at the ground was used for the vertical coordinate s. For most runs 44 points were used in a domain with depth 13.5; the grid length was 0.15 at the ground increasing monotonically to 0.50 at the lid. For runs with $\mathrm{Fr} > 2.5$ (all conducted at low Ro) the height of the lid was increased so as to keep the mountain height less than about 20% of the model depth. These simulations suffered a slight degradation of vertical resolution, though the relatively smooth vertical

structure obtaining in the low-Ro regime is likely to render this inconsequential. For runs conducted specifically to test sensitivity to the lid height, the height of the lid was doubled by adding points at the top without altering the low-level resolution.

4. Upstream influence: The nonrotating case

a. Historical review

The problem of upstream influence has a long history. Early attention centered on the hydraulic problem, consisting of flow of a thin (hence hydrostatic) layer of homogeneous fluid in a nonrotating system. A review of this work may be found in Long (1972, pp. 81–87). Suppose that a finite-area obstacle of maximum height h_m is located in a fluid layer of initial depth H_0, and that the layer is impulsively given a velocity U_0 at time $t = 0$. The nondimensional parameters controlling the subsequent evolution are the initial Froude number $F_0 = U_0/(gH_0)^{1/2}$ and the nondimensional obstacle height $B = h_m/H_0$. For B less than a certain critical value $B_{cr}(F_0)$, the upstream and downstream current is left unmodified after a long time has passed; for $F_0 < 1$ the fluid draws down symmetrically over the obstacle, while for $F_0 > 1$ the fluid draws up symmetrically over the obstacle. For $B > B_{cr}$, the steady symmetric solution ceases to exist. This situation is resolved by the "Gadarene swine" solution (see Benjamin and Lighthill, 1954; and Mark v, 13): A wave of elevation forms upstream of the obstacle and propagates upstream with time, leaving a layer of decelerated fluid between the wave front and the obstacle. The upstream surge is accompanied by a downstream-propagating wave of depression. After a sufficiently long time, the flow near the obstacle takes the form of a steady waterfall, with subcritical flow $[U/(gH)^{1/2} < 1]$ just upstream of the obstacle and supercritical flow $[U/(gH)^{1/2} > 1]$ just downstream of the obstacle. From Eqs. (38)–(40) of Long (1972) it may be inferred that when $F_0 < 1$

$$B_{cr} = 1 + \left(\frac{1}{2}\right)F_0^2 - \left(\frac{3}{2}\right)F_0^{2/3}. \qquad (4.1)$$

As $F_0 \to 1$, $B_{cr} \to 0$, but is positive otherwise. Thus, in hydraulic theory, upstream influence occurs only when the obstacle is of *finite height,* as long as $F_0 \neq 1$. Consequently the upstream surge cannot be obtained by an expansion about the limit of infinitesimal obstacle height, no matter how many terms are included. While a rigorous analytical theory of the formation of the upstream surge appears to be lacking, the phenomenology at least is well understood and the agreement between experiment and the existing theory is good.

The theoretical understanding of the continuously stratified case derives from elegant work by Benjamin (1970) and McIntyre (1972) on the *weakly nonlinear* problem. Benjamin's results are based on general conservation laws, and apply both to *nonhydrostatic* flow of a layer of homogeneous fluid with a free surface and to continuously stratified flow between rigid horizontal boundaries. The theorems require that the formation of a lee wave train propagating downstream of the obstacle be inevitably accompanied by the formation of surge of decelerated fluid propagating upstream of the obstacle. By "lee wave" here we refer to an undular motion that, given sufficient time, extends arbitrarily far downstream of the obstacle without diminution of amplitude. McIntyre explicitly calculated the upstream response for the case of a layer of fluid of constant stratification bounded above by a rigid lid. It was found that the upstream surge is generated in the tail of the lee wave train and not over the obstacle; this feature suggested that the upstream influence would disappear if the rigid lid were removed, allowing the wave to spread vertically as well as horizontally. In both calculations, the amplitude of the bore is of second order in the lee-wave amplitude. These theoretical results would imply that upstream influence can exist only when lee waves can exist. For a fixed layer depth in either the stratified or one-layer case, the lee wave-amplitude vanishes as the obstacle is made broad compared to the lee wavelength. Consequently, the upstream surge is predicted to vanish in the hydrostatic limit. While Benjamin did not make any claims concerning the unbounded, stratified case, McIntyre's theory decidedly implies that no upstream influence would be generated in hydrostatic flow in the unbounded domain, for which no lee waves can exist.

The association between upstream influence and lee waves should perhaps be disturbing in consideration of the firmly established fact that vigorous upstream surges occur in shallow-water flow over obstacles, even though the system does not support lee waves. Indeed the laboratory experiments of Baines (1977, 1979) demonstrate that the mechanism explored by Benjamin and by McIntyre is not the only—or even a particularly significant—mechanism for the generation of upstream influence in stratified flow. Baines (1977) reports two major discrepancies with the theory. First, the observed amplitude of the upstream bore is approximately first order rather than second order in the mountain height. The amplitude predicted by weakly nonlinear theory is over an order of magnitude below the observed strength. Second, no bore was detectable between the obstacle and the lee wave tail, in contrast with McIntyre's theory. The implication here is not that upstream influence is a linear phenomenon or that the theories of McIntyre and Benjamin are incorrect. Rather, it seems that the experiments were carried out in a regime in which the nonlinearities were order unity, revealing a type of upstream influence which is analogous to that found in hydraulic theory, and which is not accessible to the asymptotic analysis. As noted in Baines (1984),

the symmetric steady states in the continuously stratified problem with a lid cease to exist at a finite critical obstacle height in the same manner as the one-layer case, suggesting a Gadarene solution. The unbounded stratified case is fundamentally different in this regard. Steady states without upstream influence continue to exist for arbitrary obstacle heights; these states do, however, become unstable when the wave amplitude becomes large enough to overturn density contours.

In a subsequent set of experiments (Baines, 1979) it was found that the degree of upstream influence is determined primarily by Nh_m/U_0 (called "Fr" in the present work). The relative insensitivity of the upstream influence to NH/U, where H is the layer depth, demonstrates the unimportance of the lee waves and suggests that the upstream influence attains a nonvanishing asymptotic form in the limit of infinite layer depth. Understanding this limit is the key to understanding upstream influence in the real atmosphere.

b. *Numerical results for $f = 0$*

In the following we describe the character of upstream influence in a nonrotating system. The phenomenon appears in its clearest form in this case, and provides the foundation necessary for understanding the rotating problem. In this and subsequent sections the flow patterns will be described via the streamfunction $\psi(x, z, t)$ in the x–z plane, defined such that $u = \partial_z\psi$ and $w = -\partial_x\psi$. Generally, we will show contour plots of the perturbation streamfunction ψ', defined by

$$\psi(x, z, t) = z + \psi'(x, z, t) \tag{4.2}$$

In this definition, it is not assumed that ψ' is small. Negative values will be shown as dashed contours, minima will be indicated by the symbol L and maxima by the symbol H. The perturbation circulation follows contours clockwise around minima and counterclockwise around maxima.

In Fig. 3 we show contours of ψ' at times $t = 3.6$, 7.2, 10.8 and 14.4 after the impulsive start of flow over a mountain with Fr = 2. The calculations were done with the model lid at $z = 13.5$ and the sponge layer beginning at $z = 9$. The response is seen to consist of 1) an upstream-propagating disturbance, 2) a downstream-propagating disturbance, and 3) an upward-propagating hydrostatic gravity wave located immediately over the mountain. Only the last of these is present in the traditional picture of stratified hydrostatic flow over an obstacle.

The upstream disturbance creates a layer of decelerated fluid below mountain-top level accompanied by an accelerated jet above mountain-top level. This pattern shows no sign of dispersing in the vertical as it propagates upstream. The downstream disturbance creates a thin low-level layer of accelerated fluid accompanied by a decelerated layer centered at mountain-top height. It, too, maintains its intensity as it propagates. Stratified flow thus exhibits upstream influence of a type similar to that found in one-layer hydraulic theory; in both cases, a deep upstream-propagating layer of decelerated fluid is created in conjunction with a shallow downstream-propagating layer of accelerated fluid.

Further properties of the upstream surge are revealed in the time evolution of the ground-level wind upstream of the mountain, shown in Fig. 4. The vertical axis is distance upstream of the peak, with the peak located at the top of the figure, and the horizontal axis is nondimensional time. In this domain, we plot contours of $u(x, z, t)|_{z=h(x)}$ at contour intervals of 0.25. The decelerated region ($u < 1$) is shaded, the boundary of the most darkly shaded region corresponding to $u = 0$ and successive contours corresponding to $u = 0.25$, $u = 0.50$, $u = 0.75$ and $u = 1.00$. We will adhere to this convention for all figures of this type referred to in the subsequent discussion.

Figure 4 confirms that the obstacle creates a layer of stagnant fluid which extends progressively further upstream as time passes. It also reveals that the upstream surge is composed of waves which propagate with well-defined speeds. The contours for $u = 0.75$ and $u = 0.5$ propagate upstream with uniform speed $c = -1.06$ following some initial transience, while the contours for $u = 0.25$ and $u = 0$ propagate with speed $c = -0.39$ (at least for $t < 10$). When Fr is reduced to 1.5 the excitation of the slower disturbance is increased at the expense of the faster disturbance. This effect is evident in Fig. 5, where it is seen that the $u = 0.5$ contour is carried by the slow disturbance for the lower mountain. The reason for the discreteness of the upstream-propagating disturbances will be discussed later.

Many features of the upstream surge can be understood in terms of the dispersion relation for Boussinesq hydrostatic gravity waves. If k_z is the vertical wavenumber and k_x is the horizontal wavenumber, the frequency ω is given by

$$\omega = (U - N/k_z)k_x \tag{4.3}$$

in dimensional terms. [For the sake of economy of argument we have assumed a vertical structure proportional to $\cos(k_z z)$ or $\sin(k_z z)$, so that the two branches of the dispersion relation correspond to $k_z > 0$ and $k_z < 0$.] In terms of nondimensional variables with unit of depth U/N, (4.3) becomes

$$\omega = (1 - 1/k_z)k_x. \tag{4.4}$$

The wavenumbers for which $\omega = 0$ are particularly important, since they can be excited and maintained by steady forcing. According to (4.4) ω vanishes when $k_z = 1$, corresponding to the familiar stationary

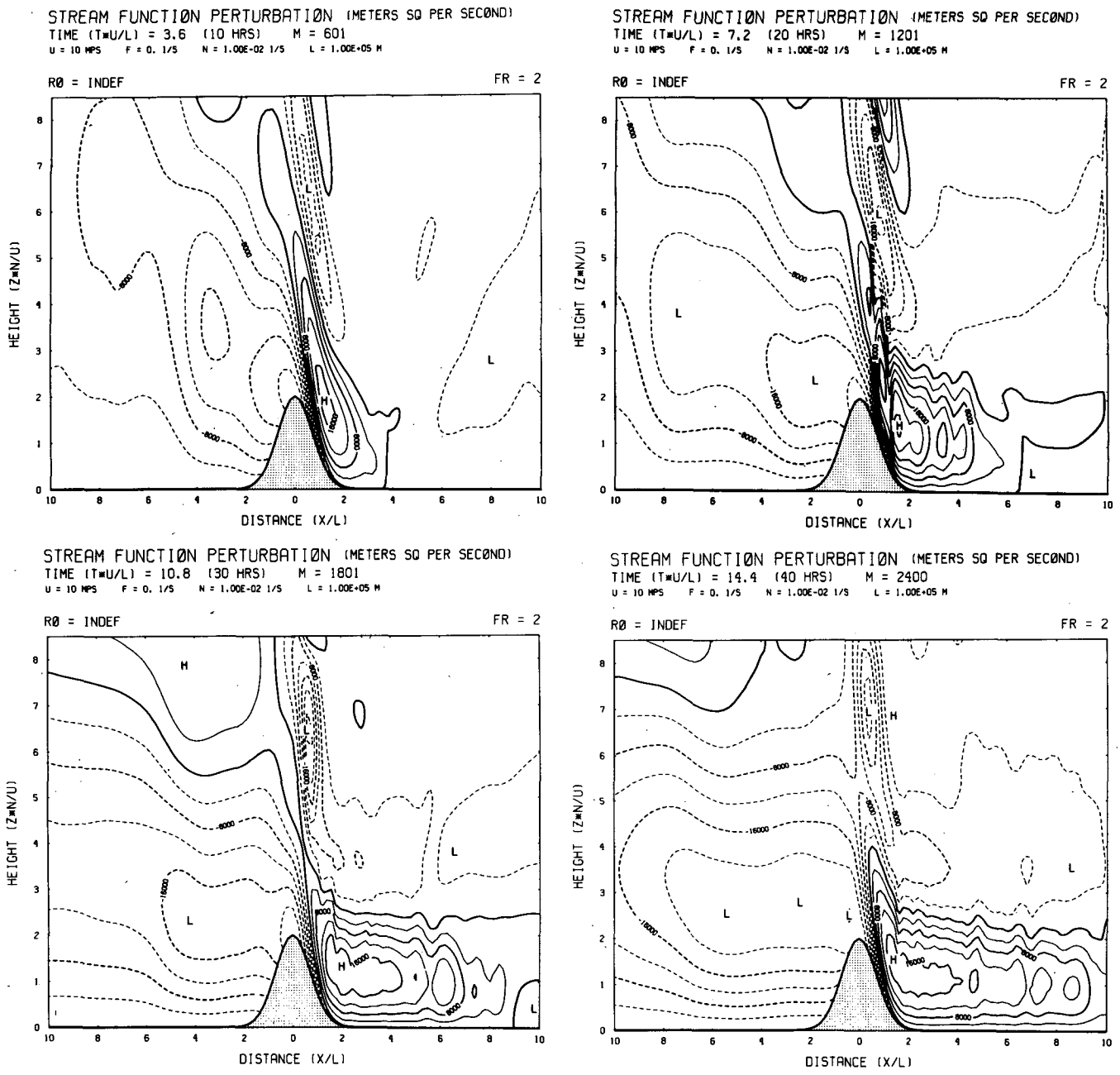

FIG. 3. Time evolution of streamfunction deviation at Fr = 2 in the nonrotating case. Nondimensional times after the impulsive startup are 3.6 (upper left), 7.2 (upper right), 10.8 (lower left) and 14.4 (lower right). Dashed contours indicate negative values. The perturbation wind circulates clockwise around minima (marked by L) and counterclockwise around maxima (marked by H).

vertically propagating gravity wave, or when $k_x = 0$, corresponding to an x-independent modification of the horizontal wind. Motions of the latter type are known as "columnar disturbances." Differentiating (4.4) and setting $k_x = 0$, we find that columnar disturbances have group velocities

$$c_{gx} = 1 - 1/k_z, \tag{4.5a}$$

$$c_{gz} = 0. \tag{4.5b}$$

Equation (4.5b) implies that columnar disturbances have purely horizontal propagation; hence they do not lose energy to $z = \infty$ as they propagate away from their source. Because the gravity waves are nondispersive in the horizontal, the temporary transients created by the impulsive startup also travel upstream and downstream with speed given by (4.5a); however, because they have nonzero vertical group velocity, these motions spread out in the vertical and

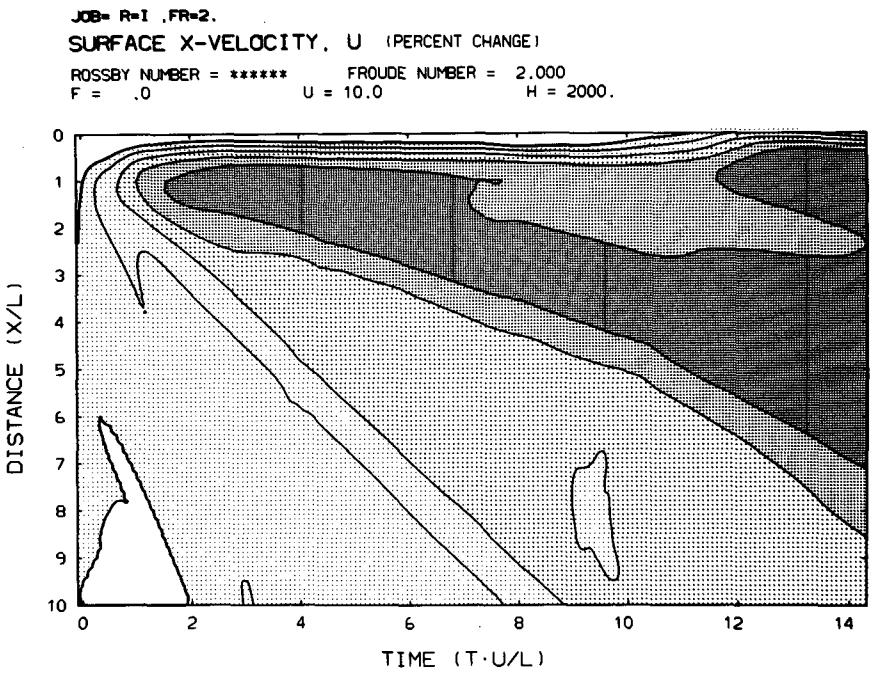

FIG. 4. Time evolution of the ground-level wind pattern upstream of the mountain for Fr = 2 in the nonrotating case. The vertical axis is distance upstream of the mountain peak, with the peak at the top of the figure. The horizontal axis is nondimensional time. In this domain are plotted contours of the cross-mountain wind u at the ground, with contour intervals 0.25. The boundary of the most darkly shaded contour corresponds to $u = 0$, and successive contours demarcate the less decelerated regions.

decay as they propagate away from the obstacle. Equation (4.5a) implies that columnar disturbances with $k_z > 1$ or $k_z < 0$ travel downstream, while disturbances with $0 < k_z < 1$ travel upstream. We tentatively identify the former with the downstream surge and the latter with the upstream surge. For a

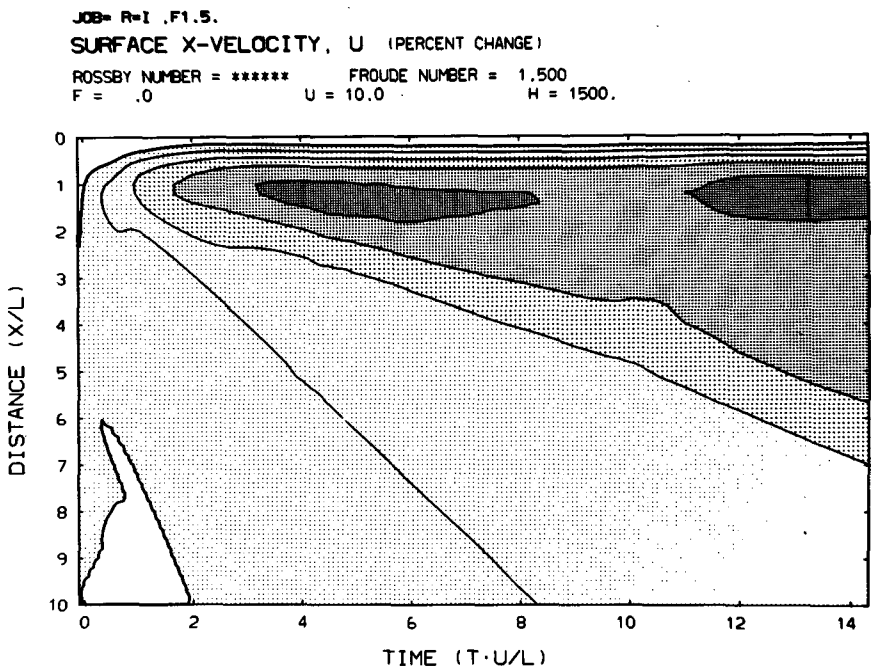

FIG. 5. As in Fig. 4 but for Fr = 1.5.

domain unbounded above, k_z can be made arbitrarily small. In the usual terminology, such a system is always subcritical, as there is always a spectrum of columnar disturbances which propagate upstream. In an unbounded domain then, the importance of upstream influence is determined by the spectrum of vertical wavenumbers which are excited with appreciable amplitude.

As discussed above, weakly nonlinear theory gives little useful insight as to the level of excitation. The numerical results and laboratory experiments point in the following direction: for sufficiently high mountains, the fundamental depth scale is the mountain height and the dominant vertical wavelength with which columnar modes are excited is proportional to this height. In nondimensional terms the dominant wavenumber $k_z = a/\mathrm{Fr}$, where a is some universal constant; according to 4.4a this disturbance moves with speed:

$$c_{gx} = 1 - \mathrm{Fr}/a. \tag{4.6}$$

Hence, when $\mathrm{Fr} > a$, an upstream columnar disturbance is efficiently excited. It follows from (4.6) that the strongly decelerated layer propagates upstream faster as the mountain is made higher. Note that in stratified flow in an unbounded domain Fr plays the dual role of determining the amplitude of the response (as seen in Section 2) and of determining the possibility of appreciable upstream propagation. In the hydraulic case these features are controlled by *two* independent parameters, B, and F_0.

The effects of columnar disturbances can be easily recognized in instantaneous plots of wind at the ground, as such disturbances create long intervals in which $u(x)$ is constant and less than unity. A convenient measure of the amplitude of a columnar disturbance is the velocity deficit $1 - u$ taken at some far-upstream point after all the disturbances have arrived. This amplitude is plotted as a function of Fr in Fig. 6. For $\mathrm{Fr} \geq 0.8$ the columnar modes were well defined by $t = 14.7$, and the amplitude $1 - u$ was determined four units upstream of the mountain peak at this time. For $\mathrm{Fr} \leq 0.7$ we found only dispersive upstream transients which eventually propagated away without substantially affecting the far-upstream flow. The amplitude jumps discontinuously to a modest value of about 0.2 as the threshold $\mathrm{Fr} = 0.75$ is crossed; as Fr is further increased, the excitation rises approximately linearly. The columnar disturbance becomes strong enough to decelerate the far-upstream surface flow to rest at about $\mathrm{Fr} = 2.0$, though values in this range were not plotted because near-mountain transience made their accurate determination impossible.

The reason for the threshold at $\mathrm{Fr} = 0.75$ is revealed in the time sequence of density and perturbation streamfunction cross sections for this value, shown in Fig. 7a, b. The key point is that $\mathrm{Fr} = 0.75$ is just slightly above the value at which wave breaking first occurs in this model. At $t = 14.4$ the density contours in the lee have just become vertical, but wave breaking has not yet set in. At this time there is a well-developed vertically propagating gravity wave over the mountain but essentially no excitation of columnar disturbances. The fact that the wave has maintained its phase tilt even though the wave front

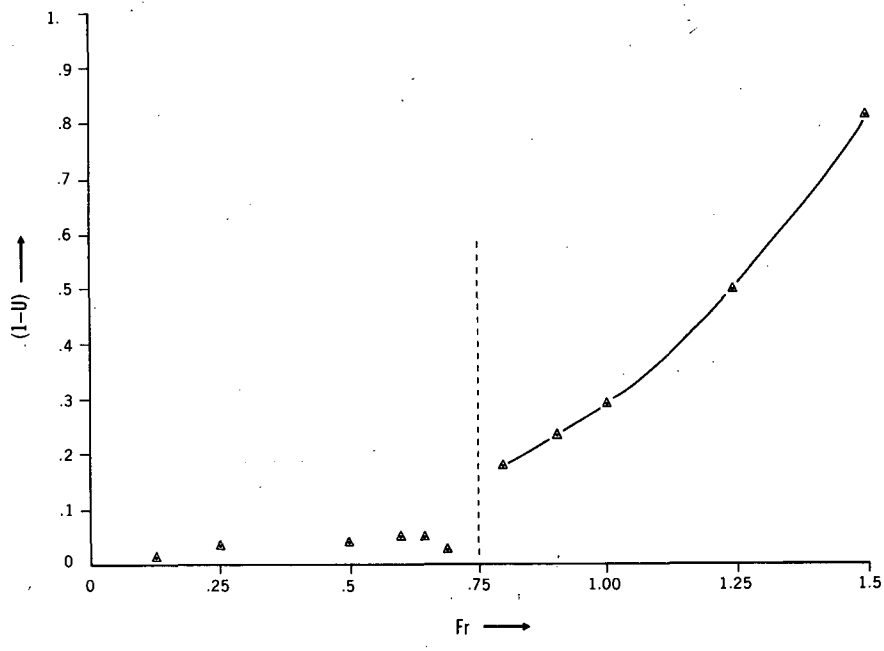

FIG. 6. Dependence of strength of the upstream surge on Fr in the nonrotating case. See text for definition of the ordinate.

reached the top well before $t = 7$ demonstrates that spurious reflection from the sponge layer is insignificant. By $t = 18$ wave breaking has begun, and the deceleration has started to extend farther upstream of the mountain. The process continues, and by $t = 25.2$ the upstream influence is clearly exhibited. There are many mechanisms by which wave breaking and the associated vertical mixing could lead to excitation of disturbances with $k_x = 0$, one candidate being the Reynolds stress convergence arising from deposition of wave pseudomomentum. An important subtlety is that in linear theory the response of the unbounded system to any forcing with a $k_x = 0$ component grows logarithmically in time without ever reaching a steady state (see Smith and Lin, 1985, for an example involving heating). These matters certainly merit further study.

In principle, one could have strong near-mountain blocking without any accompanying far-upstream influence; the near and far fields may even be controlled by physical processes that are entirely distinct. Thus the flow profiles immediately upstream of the mountain measure an independent characteristic of the flow pattern. In Fig. 8 we show $u(z)$ two units upstream of the mountain crest at $t = 14.4$ for Fr = 1, 1.5, 2 and 2.5. The fluid is decelerated below $z = 3$ and weakly accelerated above $z = 3$. Stagnant fluid appears first at the ground, when Fr = 1.5. When the mountain height is increased further, the blocked layer depth increases roughly in proportion to Fr − 1.5. This leads us to conjecture that the limiting flow for very large Fr consists of a blocked layer of sufficient depth that the layer of unblocked flow appearing just below the mountain top has thickness d such that Nd/U is approximately 1.5. The possibility of "orographic adjustment" of this sort was first suggested to us by Lindzen (personal communication, 1984). The hypothesis is consistent with the propagation characteristics of columnar disturbances: since only waves with $k_z < N/U$ can propagate upstream, the sharpest shear layer that can be constructed from such waves has a thickness of order U/N. Note that upstream blocking does not preclude strong descent in the lee, wherein fluid from above the blocked layer is entrained into the low-level turbulent wake of the mountain.

It is not certain that the near-mountain results at $t = 14$ represent true steady states. When integrated for a very long time, the system exhibited a gradual intensification of the upstream deceleration near the mountain. However, the details of this process were found to be sensitive to both the width of the model domain and the height of the model lid. Examination of the solutions suggested that the long-term evolution was caused by spurious reflections from the upstream boundary.

There appear to be no laboratory experiments carried out in a parameter range precisely analogous to that of our numerical simulations. Perhaps the closest resemblance is to be found in Baines (1979). These experiments differ from the simulations chiefly in that: 1) NL/U and h_m/L were order unity, so that the motions were not strictly hydrostatic; 2) the moderate Reynolds numbers of 300–1000 may not have been large enough to completely eliminate viscous effects; and 3) wave reflection from the effectively rigid fluid surface may have been significant. Additionally, Baines's experiments were carried out with a bell-shaped mountain $h = 1/(1 + x^2)$ instead of one Gaussian shaped. Nonetheless, the critical value Fr = 1.5 for onset of near-mountain blocking is in reasonable agreement with Baines's value Fr = 2.; we repeated the calculation for a bell-shaped mountain and found a critical Fr of 1.75, which is even closer. Another point of agreement is in the approximate linearity of the amplitude of the columnar disturbance in Fr, described in earlier experiments (Baines, 1977). Recently, Baines and Hoinka (1985) have reported on upstream influence in an apparatus contrived to simulate a radiation upper boundary condition. The upstream profiles at Fr = 2 are again similar to our simulations, though *onset* of upstream influence is found at Fr = 0.3. The discrepancy in the onset criterion may arise from nonhydrostatic effects in the laboratory experiments: since $h/L = O(1)$ in the laboratory model, NL/U is small when Fr is small, whence nonhydrostatic effects are appreciable in that regime. Given the dependence of the upstream flow on wave breaking, the consistency between laboratory and numerical experiments at the larger values of Fr is reassuring.

By effectively absorbing energy reaching the higher model levels, the sponge layer assures that the vertical confinement provided by the model lid is not necessary for upstream influence. However, the finite-depth model topped by a sponge layer does not perfectly mimic the infinite-depth system. The model does not permit a continuum of upstream-propagating columnar disturbances, as the modes in question have vertical wavelengths that are comparable to the sponge-layer thickness. In a model with rigid lid at height H without a sponge, the boundary conditions on vertical velocity require that long waves have a vertical structure in which u' is proportional to $\cos(n\pi z/H)$, where n is any integer; the corresponding horizontal group velocities are $1 - (H/n\pi)$. For $H = 13.5$, only modes with $n = 1$, 2, 3 and 4 can propagate upstream, and the last of these has negligible propagation speed. The $n = 2$ mode has speed -1.14 and the $n = 3$ mode has speed -0.43. These values are in reasonable agreement with the propagation speeds measured from Fig. 4. Evidently, the $n = 1$ mode is not significantly excited at Fr = 2. As the lid is made higher, more upstream modes are allowed and the set approaches a continuum. This effect is demonstrated in Fig. 9, where we show the Fr = 2

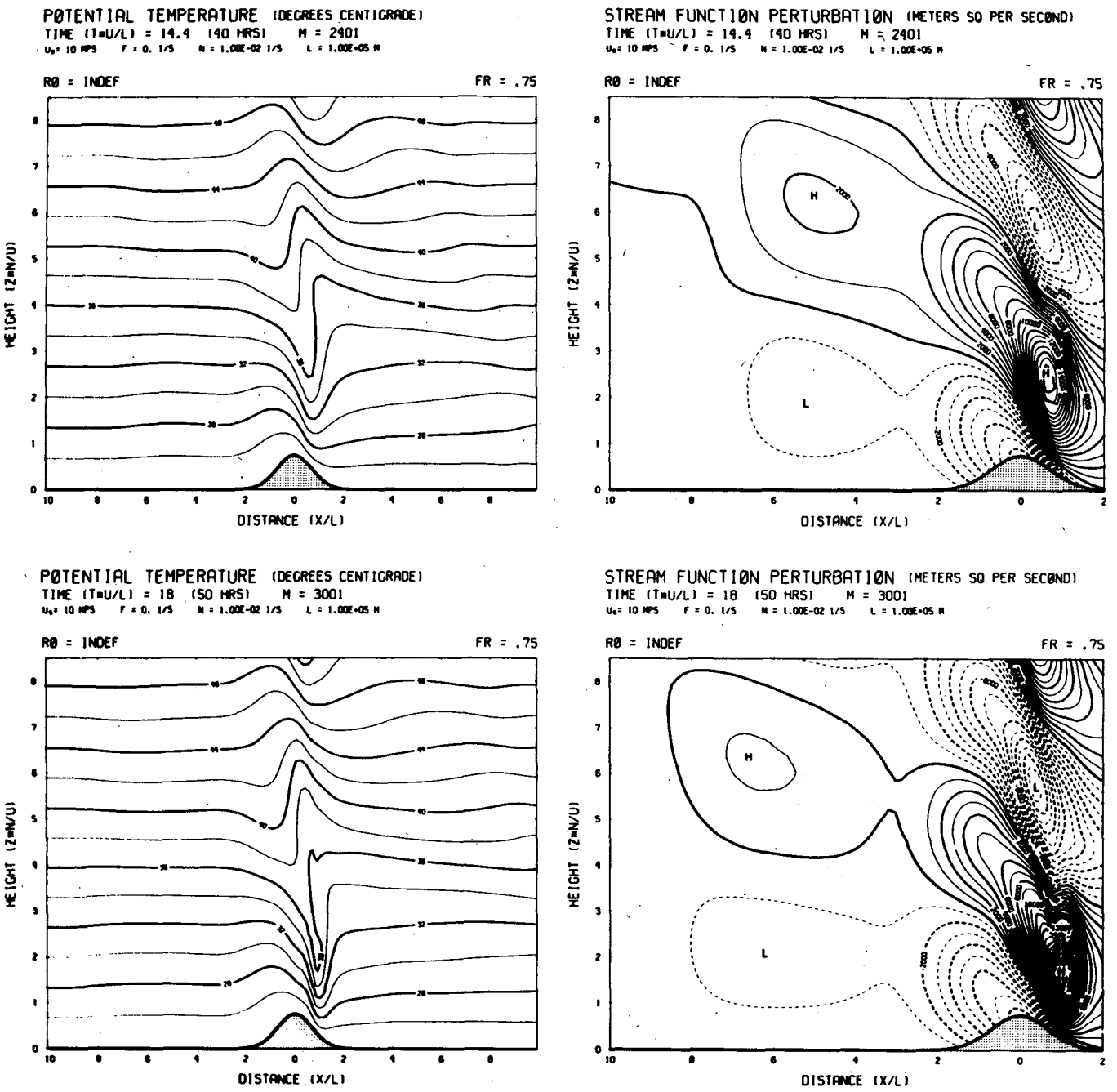

FIG. 7. Time sequence of density (left) and perturbation streamfunction (right) for Fr = 0.75. Times are 14.4 (7a, top), 18 (7a, bottom), 21.6 (7b, top), and 25.2 (7b, bottom).

time section recomputed with $H = 27$, for which depth modes $n = 1$ through $n = 8$ propagate upstream. With $N = 0.01$ sec^{-1} and $U = 10$ m s^{-1}, this depth corresponds to 27 km, whence we conclude that the details of upstream propagation in the real atmosphere are likely to be affected by winds over a very deep layer. The upstream-flow profiles, though, are not greatly troubled by this sensitivity; despite the richer spectrum of upstream-propagating modes, the near-mountain wind patterns in the high-top case (not shown) were found to be virtually identical to those shown in Fig. 8.

In summary there are three critical values of Fr for the nonrotating case: 1) Fr = 0.75, at which wave breaking and the associated excitation of upstream influence sets in, 2) Fr = 1.5, at which a stagnant region first forms near the obstacle and 3) Fr $\approx$ 2.0, at which the initial upstream surge becomes strong

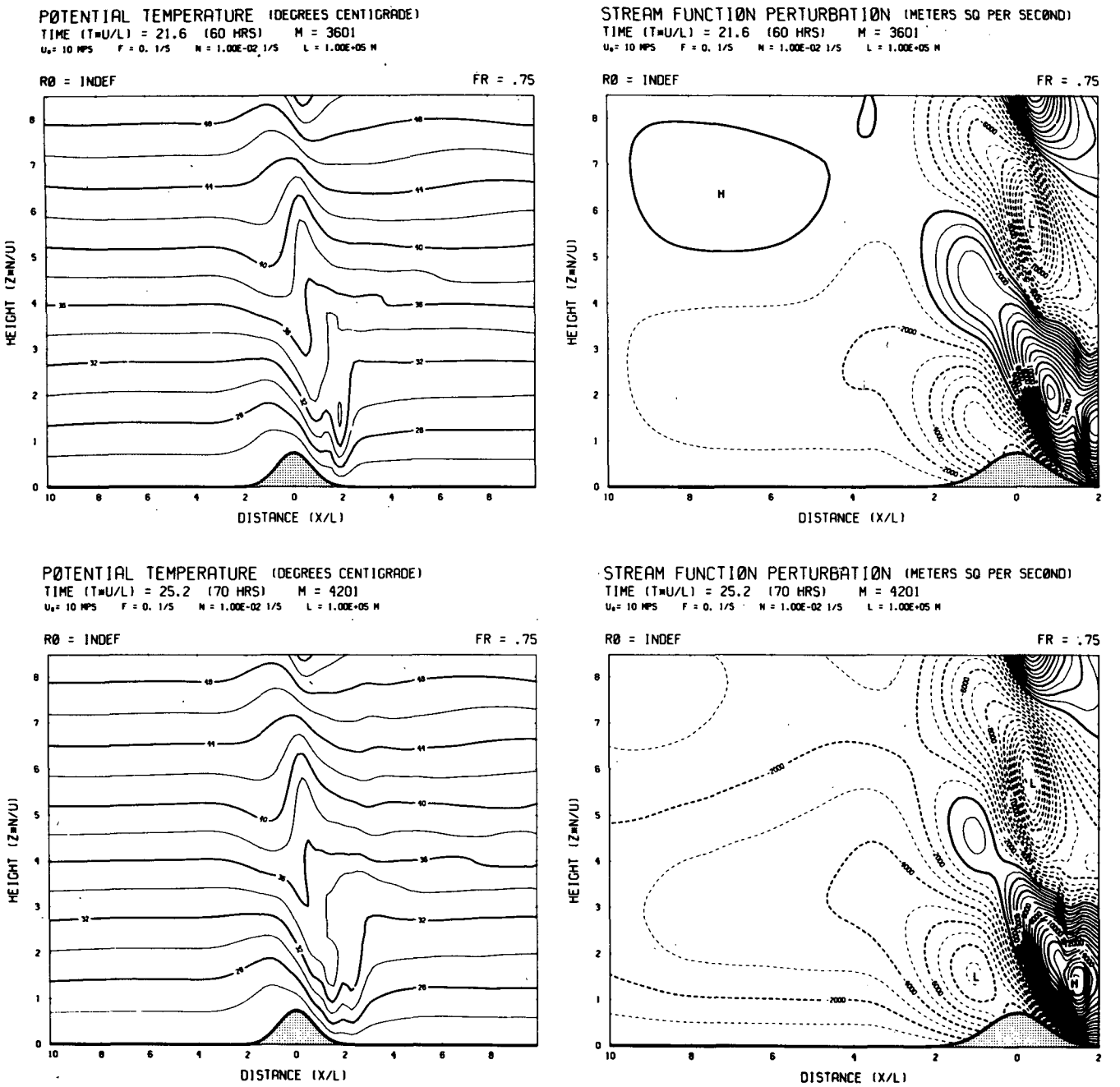

FIG. 7. (*Continued*)

enough to create a stagnant region propagating far upstream.

5. Numerical results for $f \neq 0$: The initial upstream surge

We have seen that in the nonrotating case a mountain with sufficiently large Fr generates an upstream layer of stagnant fluid that is eventually of infinite extent. In a rotating system, on the other hand, the Coriolis force would inhibit the upstream influence by forcing an adjustment to geostrophy sufficiently far upstream of the obstacle. Two simple results germane to this idea follow directly from the equations of motion. Both derive from the fact that where u is subgeostrophic the unbalanced pressure gradient in y tends to drive v positive, which in turn creates a Coriolis force in the x-direction that tends to accelerate u back toward geostrophy. The first result is as follows: in the nonrotating case the

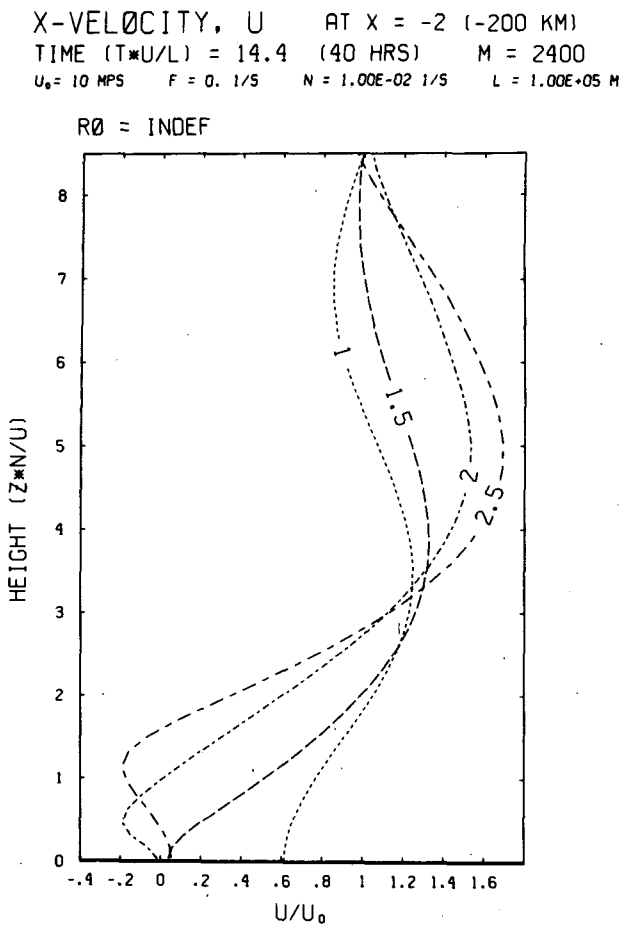

FIG. 8. Cross-mountain wind profiles two units upstream of the mountain crest in the nonrotating case as a function of Fr.

upstream surge has the effect of replacing the initial current far upstream with a modified x-independent current $u(z)$ which differs from the initial current by an order unity amount. In the rotating case, there can be no such permanent modification of the current *by any finite amount* over any stretch of fluid of nonzero length. If such a modification were to occur, the left-hand side of (2.1) would vanish because of x-independence and stationarity. Also, the pressure gradient vanishes because stationarity implies that the density is constant on streamlines, which would be horizontal under the postulated circumstance. Thus, $v = 0$ identically in the region of concern. However, (2.2) would then imply that $u = 1$ identically in this region, which proves the claim. The second result is that in a steady state u can never cross zero, provided $\partial_x v$ is finite everywhere. This follows immediately from (2.2), as the left-hand side of (2.2) vanishes where $u = 0$, which implies in contradiction that $u = 1$. Curiously, solutions in which u approaches zero and $\partial_x v$ approaches infinity near a given point are not precluded. It is easy to construct such solutions locally for a specified finite pressure gradient, though their physical relevance is not clear.

The above considerations suggest that the evolution of the rotating system should resemble that of the nonrotating system up to a dimensional time $t = O(1/f)$ ($t = O(\mathrm{Ro})$ in nondimensional units), whereafter geostrophic adjustment causes a reduction in the upstream deceleration and a retreat of the decelerated zone toward the obstacle. This conjecture is amply borne out by the simulations. In Figs. 10a–13a we show the time sections of surface wind u for

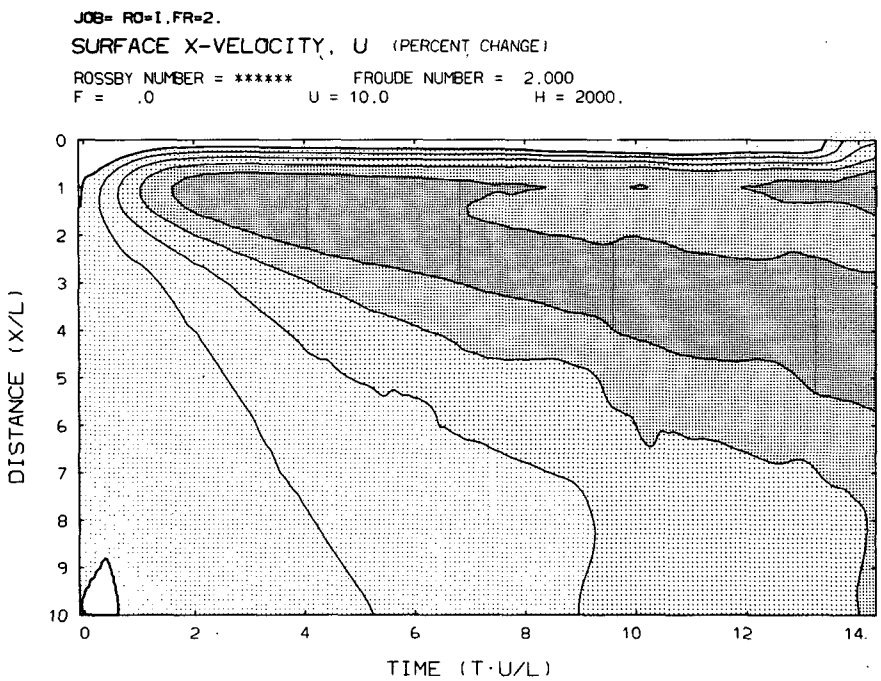

FIG. 9. As in Fig. 4 but with doubled model depth.

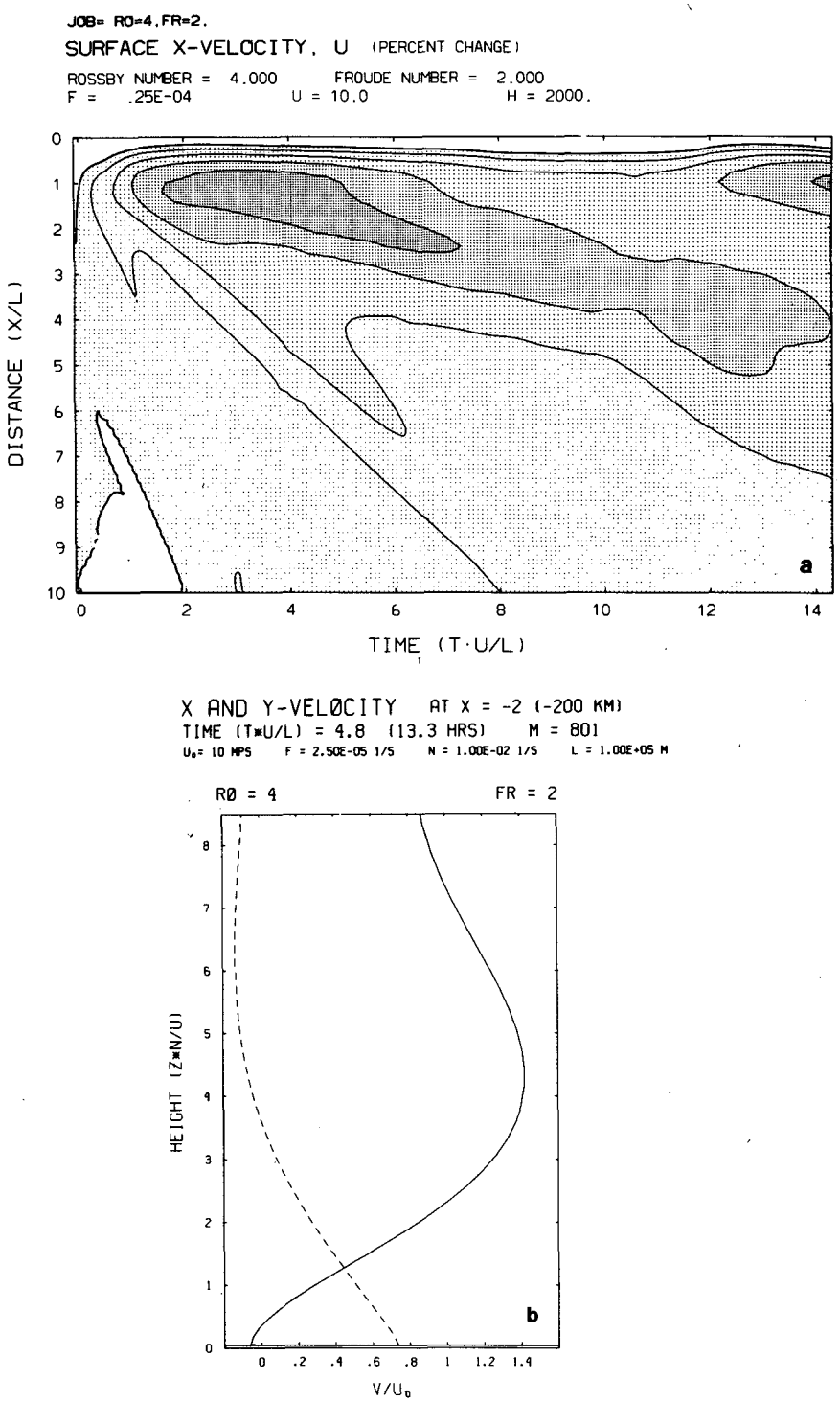

FIG. 10. (a) As in Fig. 4, but for (Ro, Fr) = (4, 2). (b) Vertical profile of cross-mountain wind (u, solid line) and along-mountain wind (v, dashed line) two units upstream of the crest at approximately the time of maximum velocity deficit.

(Ro, Fr) = (4, 2), (2, 2.5), (1, 4) and (0.25, 8). These values were chosen such that each experiment lay in the strongly nonlinear range. In each case the cross-mountain wind near the mountain falls to approximately zero before recovering to a less decelerated value. It is also evident that the upstream surge propagates only a finite distance before being arrested by geostrophic adjustment. The time scale for both

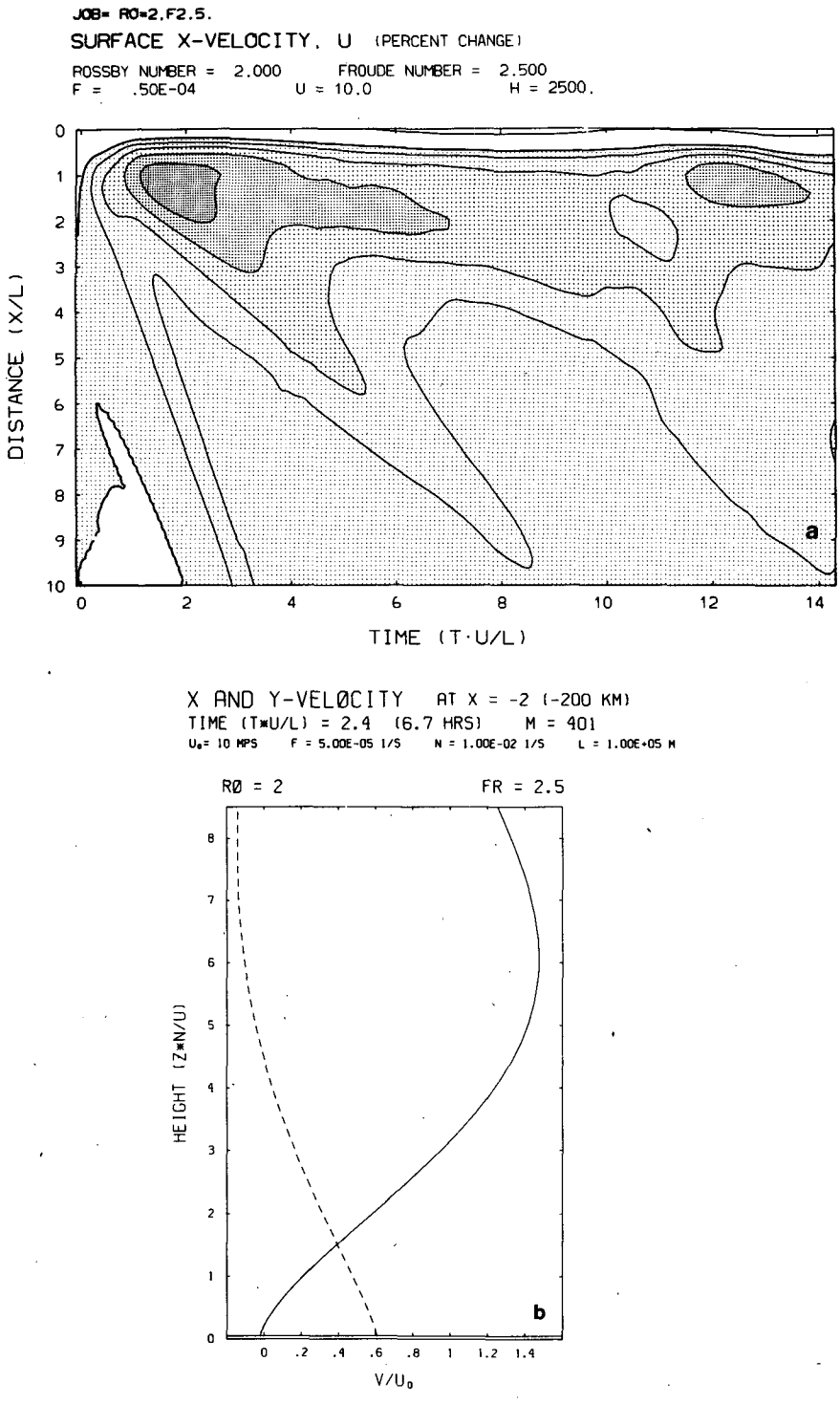

FIG. 11. As in Fig. 10 but with (Ro, Fr) = (2, 2.5).

processes becomes smaller in proportion to Ro as Ro is decreased. Recall, though, that the unit of time is L/U, so that the corresponding dimensional value remains roughly fixed at the inertial time scale; at small Ro, this time becomes small only in comparison with the time required for a fluid parcel to cross the obstacle. Thus, at small Ro the strong deceleration occurs at a time before fluid has traveled very far along the upwind slope, and likewise before there is time for a wave to develop aloft. It should also be noted that, according to the scaling arguments of Section 2, the short-time deceleration at small Ro is

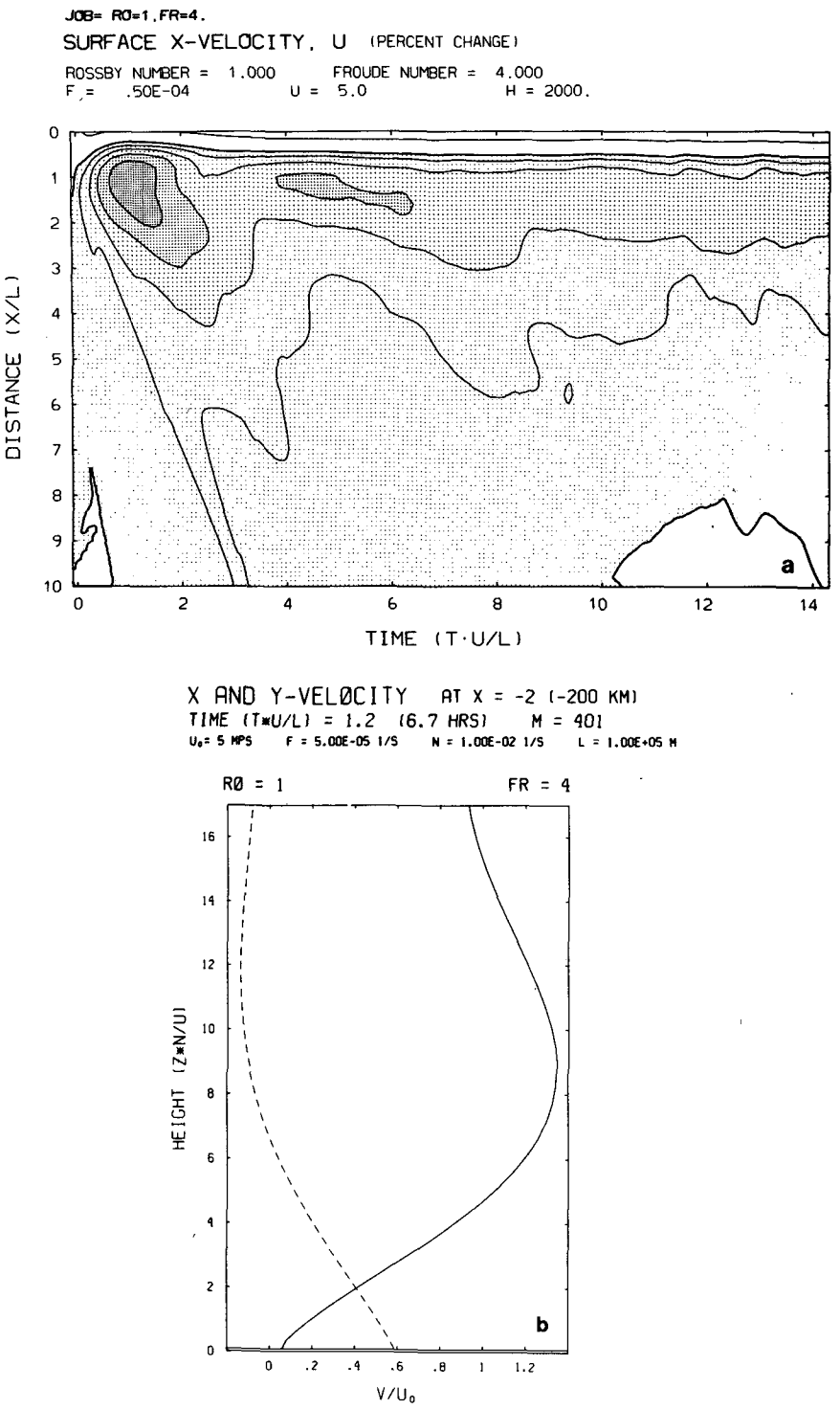

FIG. 12. As in Fig. 10 but with (Ro, Fr) = (1, 4).

an ageostrophic effect which would be missed in a balanced model.

The profiles of $u(z)$ and $v(z)$ for the aforementioned cases, taken two units upstream of the mountain peak at approximately the time of maximum velocity deficit, are shown in Figs. 10b–13b. As in the non-rotating case, the cross-mountain flow below mountain-top level is strongly decelerated while the flow above mountain-top level is somewhat accelerated. The maximum reduction occurs at the ground and, in this parameter range, decays smoothly with height. The along-mountain wind v has its maximum at the

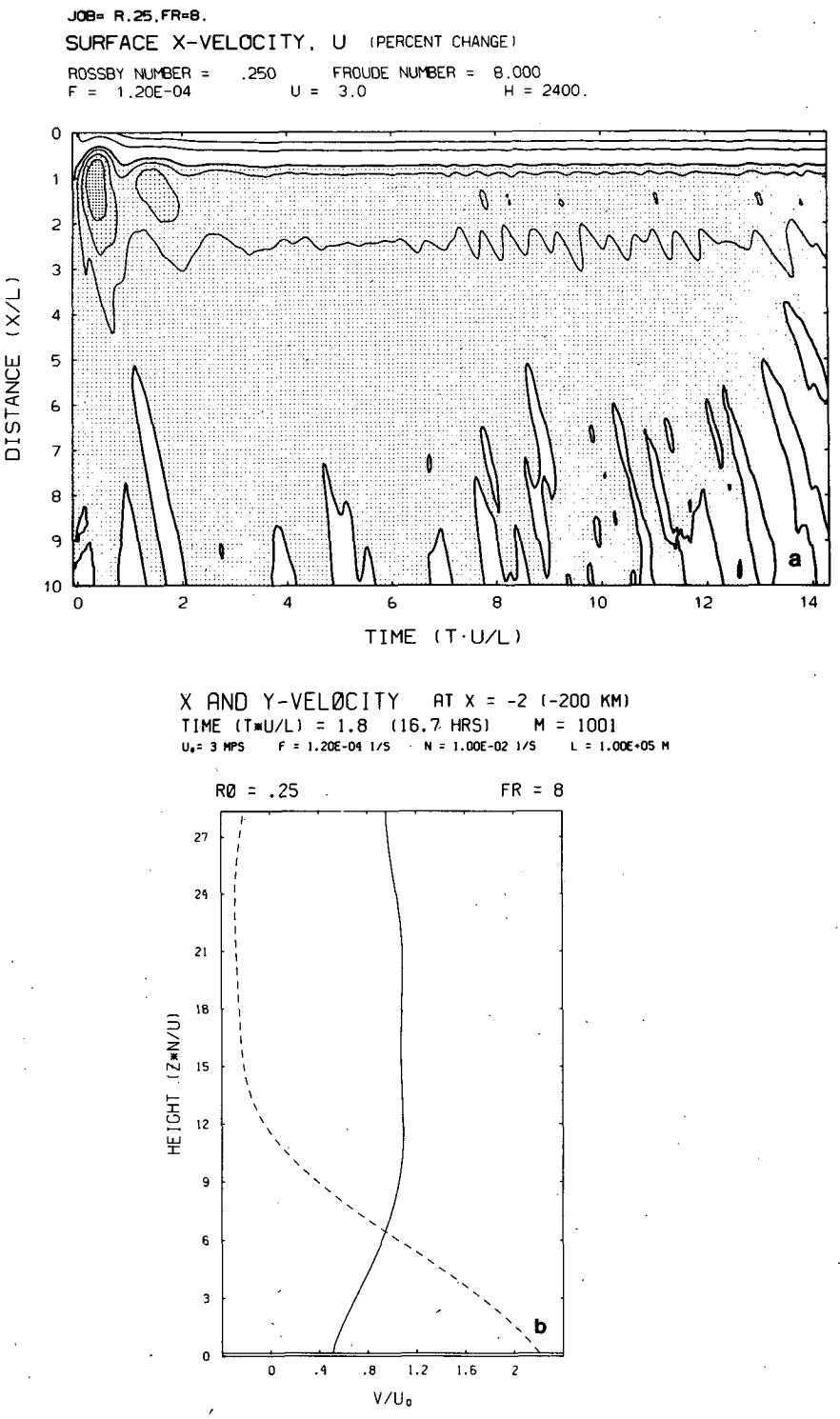

FIG. 13. As in Fig. 10 but with (Ro, Fr) = (0.25, 8).

ground, where u has its minimum, whence the associated Coriolis force tends to accelerate u. As time progresses, v continues to increase and the deceleration of u becomes less pronounced; the resulting states will be discussed in Section 6. At the time of maximum deficit, the reduction of u and acceleration of v lead to a sharp turning of the wind to the left below mountain-top level. When Ro = 2 for example, the wind turns by almost 90° between $z = 5$ and $z = 0$. It is also noteworthy that for Ro $\geqslant$ 1 the vertical

profiles are nearly identical when expressed in terms of a vertical coordinate scaled by the mountain height. This confirms the mountain height as a fundamental dynamical depth scale in the nonlinear range.

The two most important characteristics of the upstream pattern are the strength of the blocking and the length scale over which the upstream influence extends. The former is conveniently summarized by the minimum value of u (call it u_{min}) appearing anywhere upstream of the mountain crest at any time before geostrophic adjustment sets in. Contours of $(1 - u_{min})$ in the Ro–Fr plane are plotted in Fig. 14. The filled circles in the figure indicate the actual values of (Ro, Fr) for the set of simulations used in determining the contours. The shapes of the curves are in excellent agreement with the the scaling arguments given in Section 2, with the transition between the small Ro and large Ro behavior occurring near Ro = 1.

If transients in the nonrotating system propagate upstream with typical speed $1 - \mathrm{Fr}/a$, as argued in Section 4, and can continue to do so for an inertial time b Ro without being inhibited by the Coriolis force, then they should attain a maximum upstream extent dx given by

$$dx = b\,\mathrm{Ro}(\mathrm{Fr}/a - 1) = (b/a)\,\mathrm{RoFr} - b\,\mathrm{Ro}. \quad (5.1)$$

Thus, a plot of dx against RoFr should yield a straight line with intercept that shifts to the right as Ro is increased. A convenient and practical measure of dx is the distance upstream of the mountain crest at which u recovers to half the geostrophic value at the ground (call it x_{50}); this quantity is shown as a function of RoFr in Fig. 15. For purposes of reference, the line x_{50} = RoFr is also shown. The values for Ro = 0.25, 0.5 and 1.0 rise linearly in RoFr with slope near unity, though the intercept appears to remain fixed at nearly zero. For Ro = 2, 3 and 4 the apparent intercept shifts to the right with increasing Ro, in qualitative agreement with (5.1), though the upstream scales increase somewhat faster than linearly with increasing RoFr. The latter behavior may reflect the greater importance of wave breaking in generating the upstream motions when Ro is large. In light of the spurious discretization of columnar modes discussed in Section 4, one might also be suspicious of the estimates of upstream scale at the larger values of Ro, for which cases the discrete modes have sufficient time to become separated in space. Indeed, the upstream behavior for (Ro, Fr) = (4, 2) with doubled lid height shows a richer spectrum of modes (see Fig. 16). The two-stage adjustment visible in the low-top case—whereby the fast mode arrives upstream first, adjusts, and is followed by the slow mode—is absent in the high-top case. Nonetheless, the estimates of x_{50} are quite robust. The values for Ro = 4 in the high-lid case are indicated by the symbol "H" in Fig. 15, and do not reveal any great change.

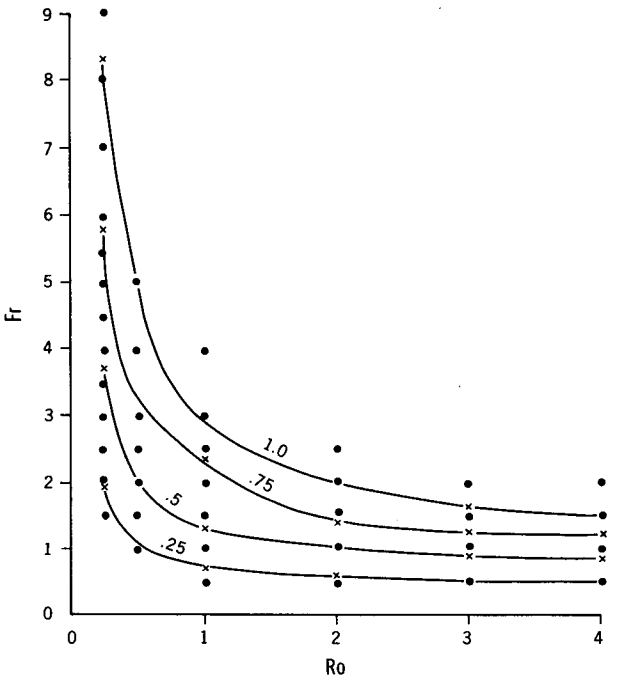

FIG. 14. Contours of the maximum deficit $(1 - u_{min})$ appearing upstream of the mountain during the initial phase, drawn in the (Ro, Fr) plane. The region of parameter space in which stagnant fluid is formed lies above the curve labeled 1.0.

These results lend some support to (5.1). To the extent that (5.1) is correct, the maximum dimensional upstream extent attained by the blocked layer scales approximately with the radius of deformation Nh_m/f when Fr is large. Since positive v is generated wherever u is appreciably subgeostrophic, this also gives the length scale over which the mountain-parallel wind extends at the end of the transient stage.

It is difficult to quantify the importance of wave breaking in generating the motions discussed above. In the nonrotating case, we could separate permanent upstream motions (presumably forced by breaking) from dispersive transients by examining the flow far upstream after a long time has passed. In the rotating case, both kinds of disturbance affect the results. Certainly wave breaking is unimportant at Ro = 0.25, for which streamlines do not overturn during the time under consideration. Wave breaking does occur for (Ro, Fr) = (2, 2.5), and no doubt influences the upstream pattern to some extent.

6. Numerical results for $f \neq 0$: Long time behavior

a. Steady states for Ro ≪ 1

Figure 13a suggests that for Ro = 0.25 the solution attains a nearly steady state after an order unity adjustment time has passed, even though the system is in the strongly nonlinear region of parameter space.

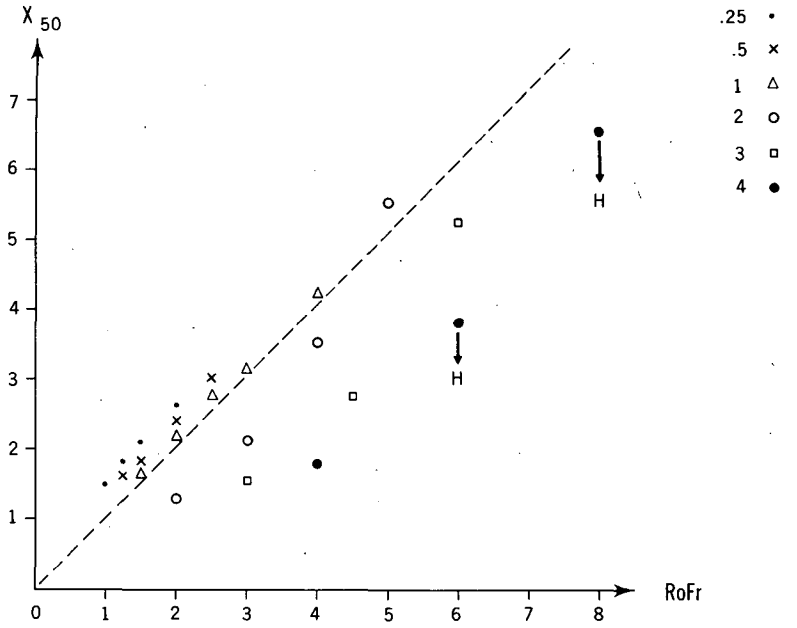

FIG. 15. Upstream extent of the 50% deceleration contour as a function of RoFr, for Ro = 0.25, 0.5, 1.0, 2.0 and 4.0. Results for Ro = 4 with a doubled model depth are indicated by "H" where there was appreciable change.

This typifies the long-term behavior at low Rossby number. In the limit of small Ro the semigeostrophic approximation is valid and steady states can be found analytically. Solutions pertinent to the geometry under consideration herein were presented by Pierrehumbert (1985b), and it is instructive to compare them with the numerical results. In semigeostrophic theory $u(x, z)$ depends only on RoFr and is symmetric about the mountain peak. At the ground the minimum velocity u_{min} is attained near the upstream and downstream feet of the mountain while the maximum velocity u_{max} is attained at the crest and becomes infinite

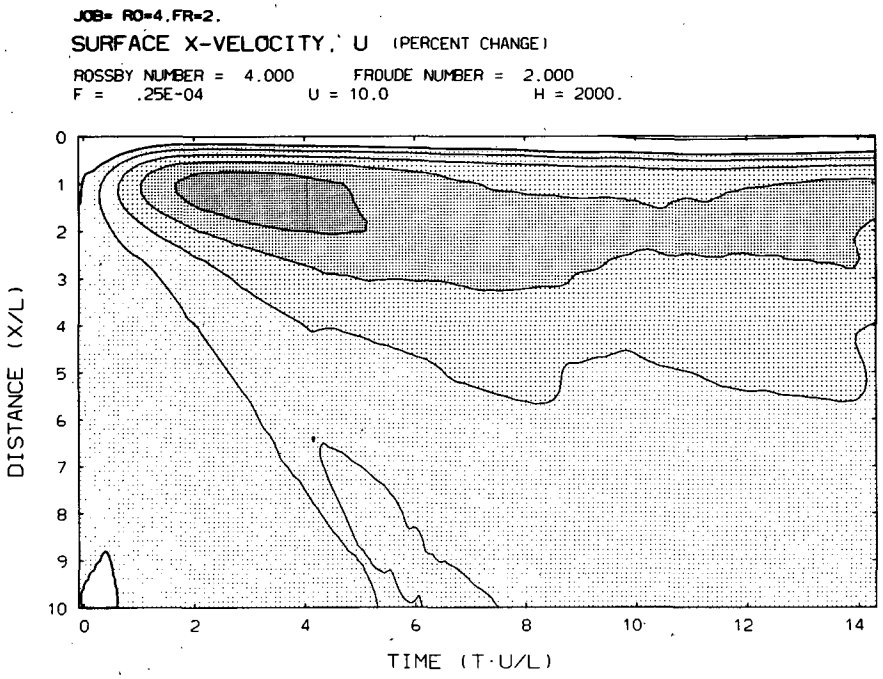

FIG. 16. As in Fig. 10a but with doubled model depth.

when RoFr = $\pi^{1/2}/2$. The theoretical results for u_{min} and u_{max} are plotted against RoFr in Fig. 17. We also show the corresponding steady numerical results for Ro = 0.25, with the solid triangles representing the minimum u appearing upstream of the mountain peak and the open triangles representing the value of u at the mountain peak. The numerical values for the wind at the peak agree with the theoretical values for small RoFr but fall below the theoretical curve as the breakdown point is approached; past this point the numerically determined peak winds increase approximately linearly in RoFr. Despite this deviation, the theoretical and numerical values for the upstream deceleration are in excellent agreement over the entire range examined, indicating that the breakdown does not affect the upstream pattern.

On the downstream side, the effects of the breakdown are dramatic. In Fig. 18 we show the steady streamfunction perturbation for RoFr = 0.375, 0.625 and 2, with Ro fixed at 0.25. When RoFr = 0.375, well below the breakdown point, the pattern is quite symmetrical and exhibits only a hint of wave radiation. At RoFr = 0.625, just below breakdown, the maximum wind shifts markedly to the downstream slope and the wave radiation becomes more pronounced. At RoFr = 2, well above breakdown, the strong, shallow current penetrates further downstream of the mountain. The sequence in Fig. 18 demonstrates the effect of the inertial terms neglected in the semigeostrophic approximation: when u becomes large near the crest the formerly negligible advection of the x-momentum becomes significant and high-momentum air is carried into the lee.[2]

We conclude that the semigeostrophic solutions continue to provide accurate estimates of the upstream deceleration at small Ro even when RoFr is considerably larger than the critical value at which the approximation breaks down near the mountain crest, as the effects of the breakdown are manifested primarily on the downstream side. The results of Pierrehumbert (1985b) then imply that the dimensional length over which the steady-state decelerated zone extends is proportional to $(LL_d)^{1/2}$, where $L_d = Nh_m/f$ is the radius of deformation. In the strongly nonlinear range (RoFr $\gg$ 1) this is considerably less than the length L_d attained by the blocked zone during the transient stage.

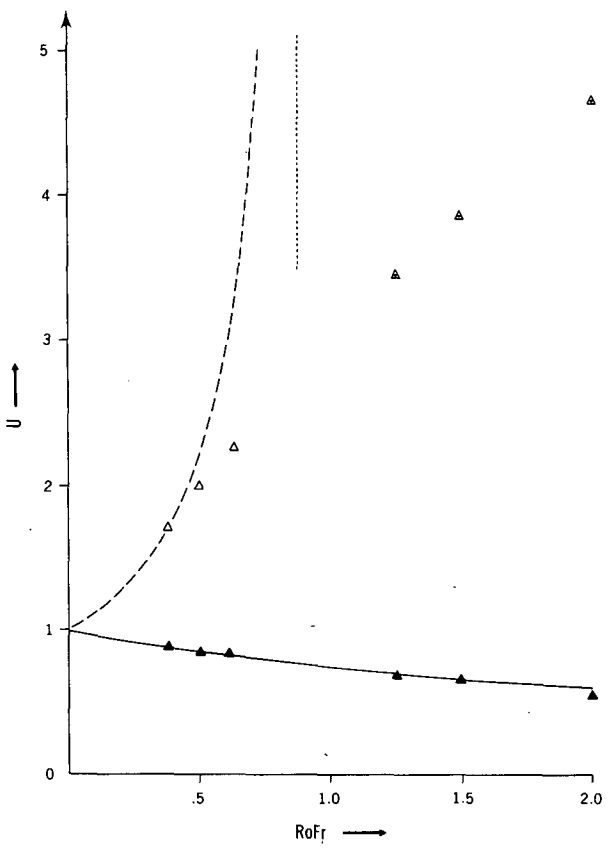

FIG. 17. Minimum velocity on upwind slope (solid line); semigeostrophic theory (solid triangles); numerical results for Ro = 0.25 and velocity at peak (dashed line); semigeostrophic theory (open triangles); numerical results as a function of RoFr.

b. *Long-term behavior for Ro $\geq$ 1*

Unfortunately, the character of the solution at long times in the ageostrophic regime is more complicated than that found in the semigeostrophic regime. In the ageostrophic regime, the system fails to reach a steady state when Fr is sufficiently large. This is apparent in Figs. 10a–12a; moreover, an integration of the Ro = 4, Fr = 2 case out to t = 57 showed that the transience does not disappear at longer times. Yet, the details of the long-term transience were found to be sensitive to model-dependent parameters, and in particular to the height of the model lid. This difficulty has prevented us from obtaining reliable estimates of the strength of the blocking or the upstream length scales in the regime Ro $\geq$ 1. We will confine ourselves here to a few comments on the qualitative nature of the flow.

The value of u at the ground two units upstream of the crest at t = 14.4 is about 0.25 in both the (Ro, Fr) = (4, 2) and (2, 2.5) cases, indicating that at long times as well as short times the cross-mountain wind is insensitive to Ro in the large Ro range. The maximum v at the same time is about 1.8 in both cases; this behavior contrasts with steady linear theory,

[2] An instance of this phenomenon may have been reported by Twain in 1872 (*RI*, p. 128). In describing a downslope wind storm in Carson City, he writes: ". . . 'The Washoe Zephr' (Washoe is a pet nickname for Nevada) is a peculiarly Scriptural wind in that no man knoweth 'whence it cometh.' That is to say, where it *originates*. It comes right over the mountains from the west, but when one crosses the ridge he does not find any of it on the other side! It probably is manufactured on the mountaintop for the occasion, and starts from there."

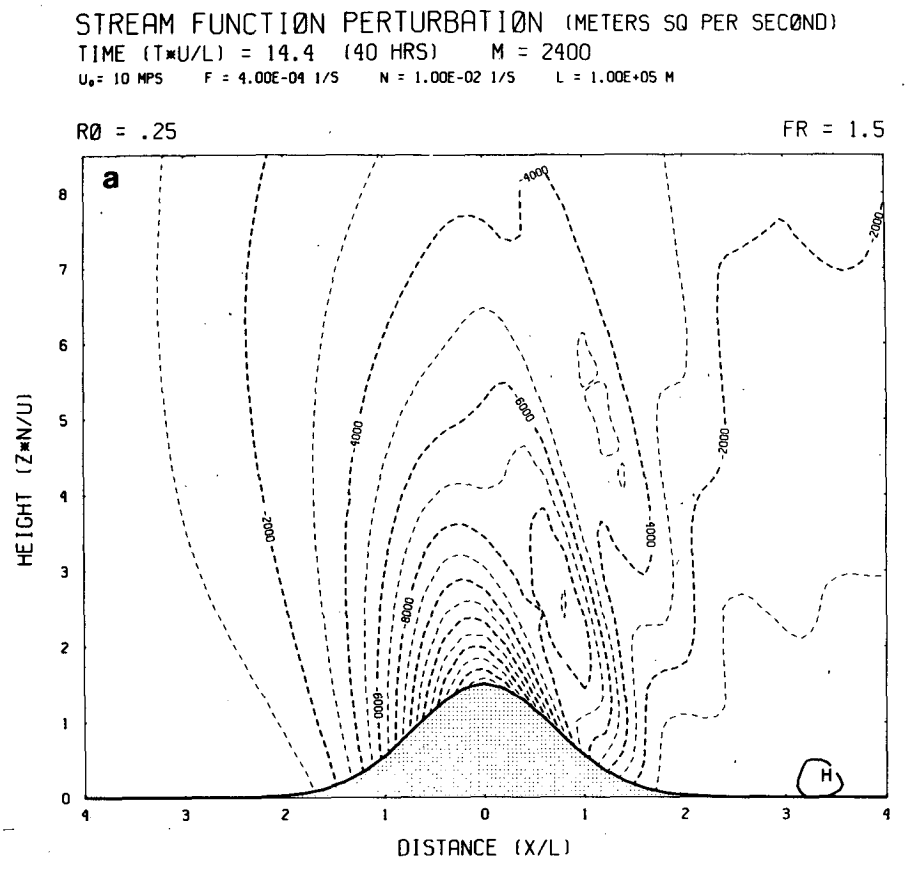

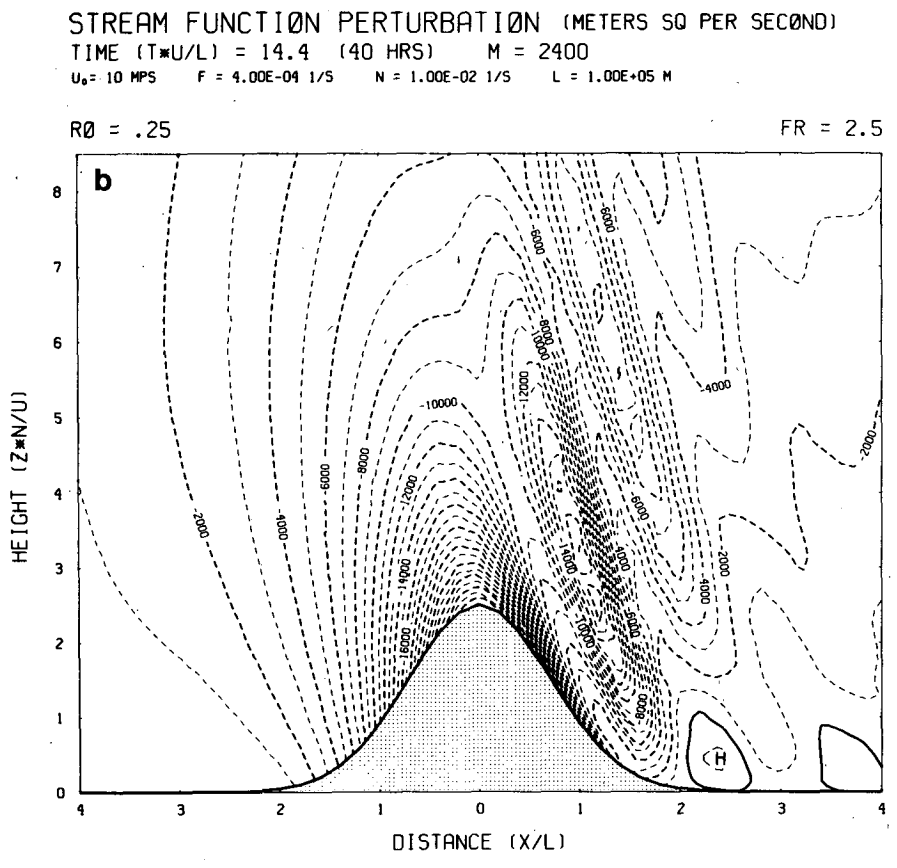

FIG. 18. Steady-state streamfunction perturbation for Ro = 0.25 with Fr = 1.5 (a), 2.5 (b) and 8 (c).

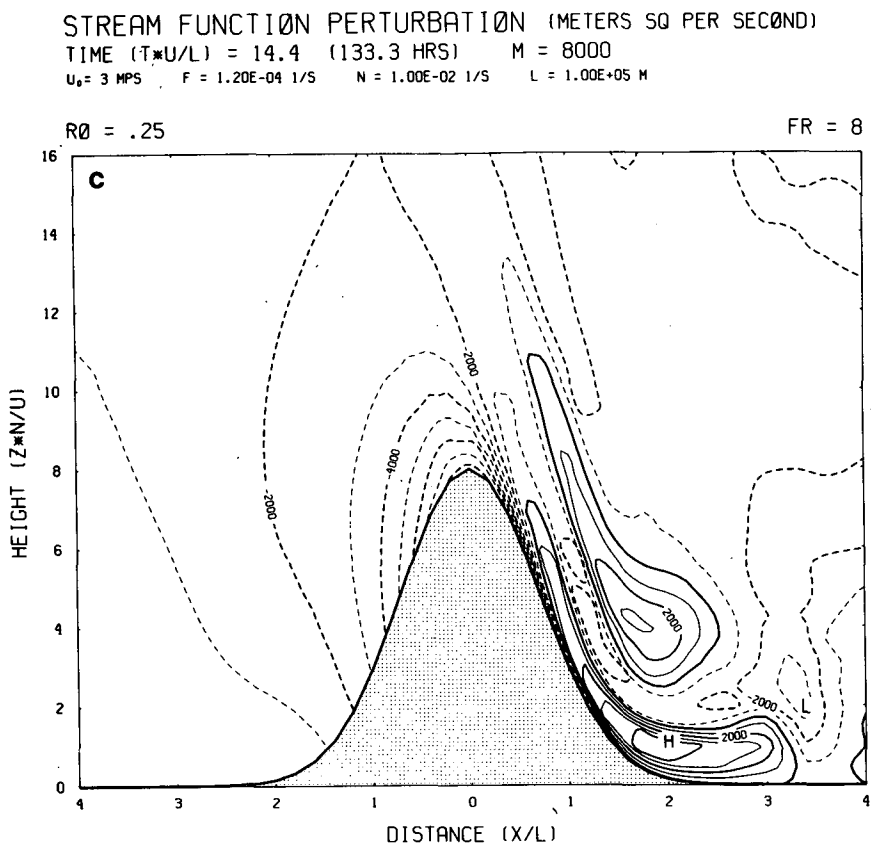

FIG. 18. (*Continued*)

for which v decreases as Ro is increased. As Ro is reduced to unity, the dependence of both winds on Ro becomes appreciable. At $t = 14.4$ in the (Ro, Fr) = (1, 4) case, the minimum u is somewhat less than 0.5 and the maximum v is about 3. Semigeostrophic theory would imply a minimum u of 0.43 when RoFr = 4, suggesting that semigeostrophic behavior remains qualitatively correct for values of Ro as large as unity.

The limit of large Ro with fixed Fr may be thought of as the "knife-edge" limit, in which the breadth of the mountain is made to vanish while keeping its height fixed. A question of particular import is whether the mountain blocks a stretch of fluid of finite length in this limit. In nondimensional units based on the mountain width, the question amounts to that of whether the upstream length scale increases linearly with Ro when Fr is held fixed.

The upstream scale must be built out of some combination of the dimensional lengths L, $L_f = U/f$ and $L_d = Nh_m/f$ (corresponding to nondimensional lengths unity, Ro and RoFr). We have seen that the upstream scale in the initial phase is probably L_d, whence a mountain affects, at least temporarily, a finite volume of fluid in the knife-edge limit. What is the corresponding answer for the long-time behavior at large Ro? In steady linear theory, the upstream flow at large Ro adjusts to geostrophy over a distance L_f, and within this distance all lengths scale with the mountain length L (Pierrehumbert, 1984); this would give a nondimensional upstream scale that is independent of Ro. In contrast, the upstream extent of the $u = 0.5$ contour toward the end of the (Ro, Fr) = (4, 2) simulation is clearly greater than that in the (2, 2.5) case. The near-mountain u and v values provide an indirect indication that the increase is nearly linear: since u and v have nearly the same magnitude near the mountain in the two cases, the subgeostrophic region must extend twice as far in the Ro = 4 case in order to yield the same v, because the nondimensional Coriolis force is Ro^{-1} times the subgeostrophic velocity. Linearity in Ro would imply an upstream length that is some combination of L_f and L_d, and because $L_d = \mathrm{Fr}L_f$, the particular combination cannot be determined without recourse to examination of the variation of the length scale with increasing Fr. Such a study must await a better understanding of the nature of the long-term transience.

7. Discussion

In the nonrotating case, a good approximation to the two-dimensional geometry can be (and has been)

realized in laboratory experiments. This may not be possible for the rotating case, as the mountain-parallel wind could lead to complicated sidewall effects. Real mountains being in any event three-dimensional, we are led to speculate on the implications of our results for the pattern of flow around a long (but not infinitely long) ridge, the long dimension of which we will denote by L_y. Consider first the nonrotating case at values of Fr large enough to produce nearly total low-level blocking. In the two-dimensional problem, the blocking propagates infinitely far upstream, but in the three-dimensional problem, the upstream influence will be limited to a distance proportional to L_y by horizontal dispersion. This is suggestive of Drazin's (1961) analytic solution for steady flow of a very strongly stratified fluid around a three-dimensional obstacle. The strong stratification suppresses vertical motion, whence the flow consists of potential flow in horizontal planes around the mountain. An identification of the long-term state with Drazin's solution upstream is also suggested by the fact that the infinite L_y limit for potential flow around a barrier consists of identically blocked flow. We thus speculate that the three dimensional pattern at large Fr attains the form shown in Fig. 19a upstream of the mountain. Our results show, on the other hand, that strong descent in the lee occurs even when the upstream flow is blocked, suggesting that potential flow would not provide a good description of the downstream flow. This is borne out by the behavior found in laboratory experiments (e.g., Baines, 1979).

In the rotating case, the Coriolis force provides an additional mechanism for limiting the extent of the upstream influence; in the transient stage, the characteristic scale is $L_d = Nh_m/f$, and in the longer term the scale is perhaps less than this. It follows that when $L_d \gg L_y$, the dominant limitation is horizontal dispersion, and again a pattern like Fig. 19a will be set up. Significantly, the low-level flow in this case is essentially nondivergent, and therefore will not be affected by the Coriolis force even in the long term.

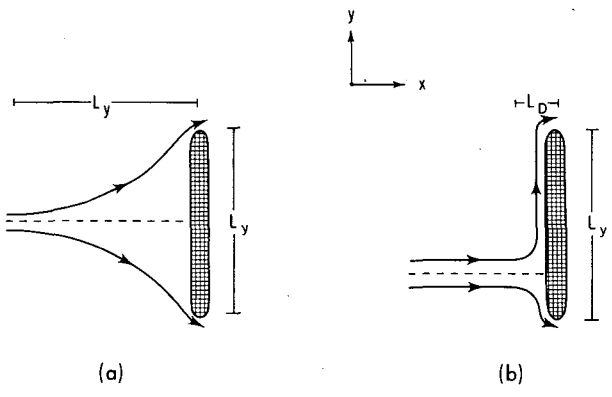

FIG. 19. Schematic three-dimensional flow patterns for $L_y \ll L_d$. (a) (potential flow in horizontal planes); (b) for $L_y \gg L_d$.

On the other hand, if a system with $L_d \ll L_y$ were impulsively started from rest, the strong upstream influence would be arrested at L_d and would never reach L_y. Within the distance L_d, the flow is subgeostrophic and the Coriolis force creates an appreciable along mountain wind, causing the fluid to flow around the mountain predominantly to the left in a pattern schematized in Fig. 19b. The barrier jet is trapped within a deformation radius of the mountain, and the situation is distinguished from potential flow by the presence of horizontal divergence, which allows the Coriolis force to be felt near the mountain.

Three dimensionality may also limit the retreat of the blocked region following the initial stage. We have seen in the two-dimensional case that u cannot be maintained at zero in a steady state. In the three-dimensional steady case, though, setting u identically zero along some line of fixed x in (2.2) implies only that

$$\partial_y(v^2/2) = 1, \tag{7.1}$$

whence we see that v accelerates in y rather than in time. The implication is that blocked air travels some distance to the left before it flows over the mountain, and if the mountain is not long enough the air could go around before it had a chance to flow over. Since v is order unity in the transient stage, which lasts a time of order Ro, the nondimensional distance traveled along the mountain during the transient stage, compared to the nondimensional length, is order $\mathrm{Ro}(L/L_y)$; since $(L/L_y) \ll 1$, there exists the possibility for air to be diverted around only in the large Ro regime, and then only if $(L_y/L) \leqslant \mathrm{O(Ro)}$. This conclusion applies only to the transient stage. In the *steady state* $v = \mathrm{O}(1/\mathrm{Ro})$, whence marked deflection of flow around the obstacle can occur at small Ro even if u is not decelerated at all.

Next, we return to the Alpine problem that motivated this work. The impulsive startup is relevant because the event shown in Fig. 1 was initiated by the arrival of a cold front, with associated strong cross-mountain winds, at the Alps six to twelve hours earlier. For the Alps, we take $L = 50$ km, $h_m = 2.5$ km, $N = 0.01$ sec^{-1} (which is consistent with upstream thermal soundings), and $f = 10^{-4}$ sec^{-1}. This yields RoFr = 5, whence the flow for small U could at best be semigeostrophic. For the 10 m s^{-1} U appropriate to the observations though, we have Ro = 2 and Fr = 2.5, which is the case shown in Fig. 11. This is well within the regime in which the low-level blocking is strong and in which the blocking persists over several hours. The values of along-mountain wind at the time of maximum blocking (about 6 m s^{-1}) are also consistent with the observations. The value of L_d is 250 km, which is rather less than the value L_y = 800 km appropriate to the Alps; thus the three-dimensional pattern is expected to be an interpolation between Figs. 19a and b. Preliminary analyses of 850

mb wind patterns appear to be consistent with this prediction.

A notable difference with the observations is that the observed wind shift is much sharper than the predicted. We believe the sharpness of the observed transition to be due to low-level convective mixing, which mixes low-velocity with higher-velocity air. The height of the shift did indeed correspond approximately to cloud-top height at the locus of the observations, and radiosonde observations away from the flight track (not shown) suggest a smoother transition. Future observational work will explore the relation between cloud distribution and wind pattern, to see if the conjecture is correct.

The surface of Earth exhibits a variety of ridgelike mountains with dimensions such that combinations of Ro and Fr similar to those found in the Alpine case would often be encountered. Accordingly, it would be expected that low-level flow diversion of the type discussed above would be a fairly common feature of flow upstream of high or steep mountains. In fact, we claim that the ubiquitous "barrier wind" phenomenon, characterized by the formation of strong winds flowing parallel to high ridges, is a manifestation of the general theory developed herein. Barrier winds have been extensively studied by Schwerdtfeger (1975), who proposed that they are a consequence of the horizontal temperature gradient created by the "damming" of low-level stable air, which implies a balanced thermal wind blowing along the barrier to the left as seen by an observer facing the barrier. This important insight is qualitatively correct in many regards, but should be considered a diagnostic description of the situation rather than a dynamical theory of the barrier wind. Schwerdtfeger's mechanism leaves unanswered the questions of the circumstances under which the blocking occurs, the length of time for which it persists and the distance upstream over which it extends. These matters cannot be treated independently of the mountain-parallel wind, as the Coriolis force couples the two horizontal wind components. Also, as we have argued in Sections 2 and 5, neither total blocking of the cross-mountain wind nor geostrophic balance of the mountain-parallel wind are necessary for the formation of barrier winds. All that is required is that u be subgeostrophic for a sufficiently long time and over a sufficiently long distance. This comment is particularly important in light of the mesoscale nature of most barrier winds.

Parish (1982) has carried out an observational and numerical study of barrier winds upstream of the Sierra Nevada Mountains. The height of these mountains attains a maximum of about 2.5 km and falls to about a third of the maximum 50 km from the peak on the windward (western) slope, whence we take $L = 50$ km. With the 10 m s^{-1} upstream flow appropriate to the 20 February 1979 case discussed by Parish we obtain Ro = 2. Parish does not give the upstream static stability, but the canonical value $N = 0.01$ s^{-1} would yield Fr = 2.5. This event is thus dynamically similar to the Alpine case, for which the appropriate numerical results are found in Fig. 11. From Fig. 11b we find that the barrier wind is only 6 m s^{-1} at the time of maximum deceleration (3.5 hours dimensionally); by 8.4 hours (results not shown), it has increased to 18 m s^{-1}, whereafter it remains somewhat steady. The latter value is consistent with the 20 m s^{-1} value found in Parish's numerical simulation, but both simulations are a bit less than the observed value of 25 m s^{-1}. In our simulations, the 50% deceleration point fluctuates between about 300 and 150 km upstream of the crest, which brackets the 220 km value observed. Parish's simulation, on the other hand, shows a decelerated layer extending more than 280 km upstream, in conflict with the observations. Nonetheless, the substantial agreement stands as an indication of the robustness of our results.

Mason and Sykes (1978, 1979) have also carried out numerical simulation of rotating, stratified flow over topography. The obstacles treated in Mason and Sykes (1979) were of very small scale [$NL/U = O(1)$]; hence the results are not relevant to the effects we have emphasized, which operate on a considerably larger scale. Broader obstacles were considered in Mason and Sykes (1978); in our notation, the values of Ro were approximately 0.1, 0.3, 1.0, and 3.0 (see Figs. 3–6 of Mason and Sykes, 1978). However, the stratified cases were all carried out with Fr = 1, which is too low to permit strong upstream blocking. For the first two cases, RoFr = 0.1 and 0.3, whence the solutions lie within the linear quasi-geostrophic regime and the streamlines are, as expected, nearly symmetrical about the crest. The Ro = 1 and Ro = 3 cases are more asymmetrical but are no less laminar, and neither exhibits much blocking. The small, shallow separation bubble found by Mason and Sykes at the upstream foot of the mountain in the latter case is absent in our calculations and may be a result of boundary layer effects.

Eliassen and Thorsteinsson (1984) report four simulations in the parameter range Ro = 1 and Fr $\leqslant$ 1. No pronounced blocking is expected in this range, and none was found. Additionally, the startup procedure was tailored to produce rapid convergence to a steady state, precluding the generation of transient upstream surges such as we have discussed.

The main implication of our results for numerical modeling—that smoothing reduces blocking—are precisely the same as discussed in Pierrehumbert (1984b) because that discussion depended only on the shape of the curves exhibited in Fig. 14. An additional implication of the nonlinear results is that a mountain creates an upstream region of relatively stagnant air that can have volume considerably greater than that of the mountain; in the transient stage, e.g.,

the stagnant region has cross-sectional area $h_m L_d = (N/f)h_m^2$, which is quadratic in the mountain height. The "effective volume" of the mountain would then be greatly reduced by smoothing. This effect may imply that use of smoothed mountains in numerical models underestimates the generation of vorticity during lee cyclogenesis and the driving of Rossby waves.

Our results may find application in a number of other orographic effects, such as the commonly observed damming of cold air east of the Appalachians and associated coastal frontogenesis (S. Garner, personal communication, 1984). In addition, although we have emphasized upstream effects, the strongly nonlinear effects considered herein also lead to considerable downslope wind amplification; the wind pattern is not too different from that expected in hydraulic theory, and yet appears in a uniformly stratified current. Such currents may play a role in severe downslope windstorms such as the Yugoslavian Bora.

8. Conclusions

We have explored the nature of impulsively started flow of a rotating, continuously stratified fluid over a ridgelike obstacle, with the intent of isolating the circumstances in which the obstacle causes substantial blocking of the oncoming flow. The controlling parameters are $\mathrm{Fr} = Nh_m/U$ and $\mathrm{Ro} = U/fL$, where N is the Brunt–Väisälä frequency, h_m the maximum mountain height, U the speed of the oncoming flow, f the Coriolis parameter and L is the half-width of the mountain. In the nonrotating limit ($f = 0$), Fr is the sole parameter, and the following results were obtained:

1) Scale analysis predicts strong blocking when $\mathrm{Fr} \geqslant \mathrm{O}(1)$.

2) Numerical simulations reveal that flow near the upstream foot of the mountain is decelerated to rest whenever $\mathrm{Fr} \geqslant 1.5$. The depth of the stagnant layer increases as Fr is made larger than the critical value.

3) When $\mathrm{Fr} > 0.75$, an upstream-propagating disturbance is formed which leaves behind a low-level layer of decelerated fluid extending arbitrarily far upstream with the passage of time. The strength of the disturbance increases monotonically as Fr is increased beyond 0.75, and becomes strong enough to create stagnant fluid when $\mathrm{Fr} = 2$. The upstream surge appears to be generated by processes associated with wave breaking above the mountain, and does not depend on downstream lee-wave trains or vertical confinement for its existence.

4) The character of the flow at $\mathrm{Fr} = 2$ is consistent with laboratory experiments conducted by Baines (1979) and Baines and Hoinka (1985).

In the rotating case, scale analysis predicts that the upstream deceleration is O(Fr) for large Ro and O(RoFr) for small Ro. The upstream cross-mountain velocity reaches a minimum within an inertial period, whereafter it recovers to a less decelerated value, owing to the action of the Coriolis force. The minimum wind in the transient phase has been determined as a function of Ro and Fr (Fig. 14), and is in excellent agreement with the scale analysis; the transition between large and small Ro behavior occurs near $\mathrm{Ro} = 1$. The Coriolis force also limits the upstream extent of the decelerated layer; in contrast with the nonrotating case, this layer attains a maximum length on the order of the radius of deformation Nh_m/f before receding back toward the mountain. Thus, the Coriolis force emerges as the major factor limiting the strength and upstream extent of flow blocking. Were it not for the Coriolis force, extensive mountain ranges would create layers of blocked fluid reaching hundreds or even thousands of kilometers upstream.

For small Ro, the solution settles into a steady state following the transition phase described above. The upstream pattern in this state is well described by semigeostrophic theory, even when RoFr is larger than the critical value at which the approximation breaks down at and downstream of the mountain crest. In the regime $\mathrm{Ro} \geqslant 1$, there is evidence of persistent transience, and we have not yet succeeded in accurately characterizing the nature of the long-term flow in this range.

The precise role of wave breaking in generating upstream influence remains obscure. Although it seems clear that the onset of upstream influence in the nonrotating case is associated with wave breaking, the physical mechanism responsible for excitation of the columnar disturbances has not been identified. It also remains to be seen whether excitation mechanisms independent of wave breaking become operative at large Fr. In the rotating case, the extent to which the transient upstream motions depend on wave breaking has yet to be determined.

The Alpine case that motivated the study described herein was found to lie in a parameter regime in which strong blocking is expected, though the comparison between theory and observation must be regarded as tentative pending a more detailed examination of the data than has been attempted here. Certain key features of the observations are accounted for by the theory, but the theory does not reproduce the sharpness of the wind shift seen in the vertical soundings; it is suggested that this sharpness is due to low-level convective mixing. The theory is also consistent with earlier observations and numerical simulations of barrier winds, in particular upstream of the Sierra Nevada Mountains.

The model considered here reproduces the phenomenon stripped to its essentials, but many extensions must be made before the complications obtaining in realistic situations can be treated. Even within

the two-dimensional geometry, the effects of vertical shear, nonuniform stratification, and more realistic initiation (e.g., frontal passage) need to be explored. Three-dimensional simulations need to be conducted in order to test the conjectures presented in Section 7; such work would also seem necessary to probe the effects of an ambient wind which changes direction with height. Finally, much analysis of the ALPEX data will be required in order to better define the phenomenon and provide rigorous tests of theories seeking to explain it.

Acknowledgments. The authors are indebted to Lee-Or Merkine and Peter Bannon for brief but illuminating discussions concerning the matters treated herein, and to Isidoro Orlanski and Bruce Ross for the use of their numerical model. The participation of R.T.P. in the Alpine Experiment and much exploratory work leading to the results presented above were made possible by a grant from the National Science Foundation (81-15394-ATM).

REFERENCES

Baines, P., 1977: Upstream influence and Long's model in stratified flows. *J. Fluid Mech.*, **82,** 147–159.

——, 1979: Observations of stratified flow past three-dimensional barriers. *J. Geophys. Res.*, **84,** 7834–7837.

——, 1984: A unified description of two-layer flow over topography, *J. Fluid Mech.*, **146,** 127–167.

——, and K. P. Hoinka, 1985: Stratified flow over two-dimensional topography in fluid of infinite depth—A laboratory simulation. *J. Atmos. Sci.*, (to be published).

Benjamin, T. B., 1970: Upstream influence. *J. Fluid Mech.*, **40,** 49–79.

——, and M. J. Lighthill, 1954: On cnoidal waves and bores. *Proc. Roy. Soc. London,* **A224,** 448–460.

Drazin, P. G., 1961: On the steady flow of a fluid of variable density past an obstacle. *Tellus,* **13,** 239–251.

Eliassen, A., and J. A. Rekustad, 1971: A numerical study of mesoscale mountain waves. *Geofys. Publ.*, **28**(3), 1–13.

——, and S. Thorsteinsson, 1984: Numerical studies of stratified air flow over a mountain ridge on the rotating earth. *Tellus,* **36,** 172–186.

Lilly, D. K., and J. B. Klemp, 1979: The effects of terrain shape on nonlinear hydrostatic mountain waves. *J. Fluid Mech.*, **95,** 241–261.

Long, R., 1972: Finite amplitude disturbances in the flow of inviscid rotating and stratified fluids over obstacles. *Annual Reviews in Fluid Mechanics,* Vol. 4, Annual Reviews, 69–92.

Mason, P. J., and R. I. Sykes, 1978: On the interaction of topography and Ekman boundary layer pumping in a stratified atmosphere. *Quart. J. Roy. Meteor. Soc.,* **104,** 475–490.

——, and ——, 1979: Separation effects in Ekman layer flow over ridges. *Quart. J. Roy. Meteor. Soc.,* **105,** 129–146.

McIntyre, M., 1972: On Long's hypothesis of no upstream influence in uniformly stratified or rotating flow. *J. Fluid Mech.*, **52,** 202–243.

Merkine, L. O., 1975: Steady finite-amplitude baroclinic flow over long topography in a rotating stratified atmosphere. *J. Atmos. Sci.*, **32,** 1881–1893.

Orlanski, I., and B. B. Ross, 1977: The circulation associated with a cold front. Part I: Dry case. *J. Atmos. Sci.*, **34,** 1619–1633.

Parish, T. R., 1982: Barrier winds along the Sierra Nevada Mountains. *J. Appl. Meteor.*, **21,** 925–930.

Peltier, W. R., and T. L. Clark, 1979: The evolution and stability of finite-amplitude mountain waves. Part II: Surface wave drag and severe downslope windstorms. *J. Atmos. Sci.*, **36,** 1498–1529.

Pierrehumbert, R. T., 1984: Linear results on the barrier effects of mesoscale mountains. *J. Atmos. Sci.*, **41,** 1356–1367.

——, 1985a: Formation of shear layers upstream of the Alps. *Rev. Meteor. Aero.*, (to be published)

——, 1985b: Stratified semigeostrophic flow over two-dimensional topography in an unbounded atmosphere. *J. Atmos. Sci.*, **42,** 523–526.

Queney, P., 1947: Theory of perturbations in stratified currents with application to airflow over mountain barriers, University of Chicago Misc. Rep. No. 23, 81 pp.

Schwerdtfeger, W., 1975: The effect of the Antarctic Peninsula on the temperature regime of the Wedell Sea. *Mon. Wea. Rev.*, **103,** 45–51.

Smith, R. B., and Y. Lin, 1985: The transient dynamics of airflow near a local heat source. *J. Atmos. Sci.*, (submitted).

Twain, M., 1872: *Roughing It,* Chap. XXI, New American Library, 448 pp.